NASA TN D-1255

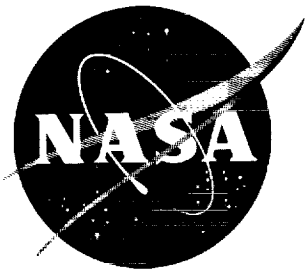

TECHNICAL NOTE

D-1255

LOW-SPEED WIND-TUNNEL INVESTIGATION TO DETERMINE THE FLIGHT CHARACTERISTICS OF A MODEL OF A PARAWING UTILITY VEHICLE

By Joseph L. Johnson, Jr.

Langley Research Center
Langley Station, Hampton, Va.

NATIONAL AERONAUTICS AND SPACE ADMINISTRATION
WASHINGTON August 1962

NATIONAL AERONAUTICS AND SPACE ADMINISTRATION

TECHNICAL NOTE D-1255

LOW-SPEED WIND-TUNNEL INVESTIGATION TO DETERMINE THE FLIGHT CHARACTERISTICS OF A MODEL OF A PARAWING UTILITY VEHICLE

By Joseph L. Johnson, Jr.

SUMMARY

A low-speed wind-tunnel investigation has been made to determine the flight characteristics of a model of a parawing utility vehicle. Flight tests were made over an angle-of-attack range of the parawing keel from about 17° to 40°. The model consisted basically of a cargo platform attached to a parawing by means of an overhead truss arrangement and was powered by a pusher propeller located at the aft end of the platform. The parawing was of extremely lightweight construction and was attached to the support structure through a universal joint so that it could be pitched or rolled for control. The flexibility resulting from the lightweight construction led to considerable deflection of the parawing members with aerodynamic loading.

The results of the investigation showed that the model had generally satisfactory longitudinal and lateral stability characteristics over the angle-of-attack range investigated. The control system used on the model proved to be generally satisfactory (except for lateral control at high angles of attack), but these results do not take into account stick forces which the analysis of this investigation has shown could be objectionable in a configuration of this type. The lateral control provided by rolling the wing was satisfactory in the lower angle-of-attack range investigated (keel angles of 17° to 25°) but this control became progressively weaker with increasing angle of attack until at angles of attack of the keel above about 35° it appeared to be ineffective. Use of a rudder mounted behind the pusher propeller to provide favorable yawing moments resulted in satisfactory flights to a keel angle of attack of 40° when the rudder was coordinated with the wing control. Because of the high effective dihedral in the high angle-of-attack range, satisfactory flights could also be made by using the rudder alone for control.

INTRODUCTION

The National Aeronautics and Space Administration is conducting a general investigation to provide some basic information on configurations employing the parawing concept. (For example, see refs. 1 to 3.) As part of this general study, a low-speed flight-test investigation has been conducted in the Langley full-scale tunnel on a model of a parawing utility vehicle. The model consisted basically of a cargo platform attached to a parawing by means of an overhead truss arrangement. The vehicle was powered by a pusher propeller located at the aft end of the platform and had a cockpit located at the front. The parawing was attached at the apex of the support structure and was gimbaled so that it could be pitched or rolled with respect to the platform for control. The configuration tested was generally similar to the Ryan flexible-wing utility airplane which has been proposed as a test vehicle to demonstrate flight characteristics of the parawing concept, as well as to provide a prototype manned combat utility vehicle. The present investigation was made to determine the dynamic stability and control characteristics of such a configuration.

Since parawing configurations are subject to deformation of fabric, keel, and leading-edge members with aerodynamic loading, it is difficult to predict the aerodynamic characteristics of a particular parawing configuration based on force-test measurements of other parawings unless such factors are closely duplicated. The parawing used in the present investigation was constructed of extremely lightweight materials without regard to specific structural considerations. For this reason, the results of this investigation are probably not directly applicable to the full-scale Ryan vehicle or to other parawing configurations having different flexibility characteristics. It is believed, however, that the results are sufficiently accurate to provide a qualitative indication of the overall flight characteristics of a configuration of this type.

Flight tests were made over an angle-of-attack range of the parawing keel from about 17° to 40°. The model was flown by using the wing to provide longitudinal and lateral control and in some instances a rudder was installed to supplement the lateral control. No consideration was given to the influence of stick forces on the dynamic control characteristics of the model in this investigation. Because of the unusual nature of the parawing utility vehicle investigated, however, a preliminary analysis of the hinge-moment and stick-force characteristics involved in a configuration of this type was made. The results of this analysis are presented in the appendix.

Static force tests were also made over a keel angle-of-attack range from 0° to 50° to determine the static stability and control characteristics of the model for correlation with the flight-test results.

SYMBOLS

All forces, moments, and velocities with the exception of lift and drag are presented with respect to a system of body axes originating at the reference center-of-gravity position shown in figure 1 unless otherwise noted. All measurements are reduced to standard coefficient form and are based on the dimensional characteristics of the fully developed wing (45° leading-edge sweep).

X,Y,Z	longitudinal, lateral, and normal body axes, respectively
x,z	distances along X- and Z-body axes, ft
x_k, z_k	distances parallel and perpendicular to parawing keel, respectively, ft,
S	wing area, sq ft
b	wing span, ft
c_k	keel length, ft
V	free-stream velocity, fps
q	free-stream dynamic pressure, lb/sq ft
α_k	angle of attack of keel, deg
α_p	angle of attack of platform, deg
i_w	angle of incidence of parawing keel angle with respect to platform, $\alpha_k - \alpha_p$, deg
β	angle of sideslip, $-\psi$, deg
ψ	angle of yaw, deg
ϕ	angle of roll, positive right wing tip down, deg
δ_r	deflection of rudder surface, positive trailing edge left, deg
F_L	lift, lb
F_D	drag, lb

L/D	lift-drag ratio
F_X	axial force, lb
F_Y	side force, lb
T	thrust, lb
M_Y	pitching moment, ft-lb
M_{Y_o}	pitching moment at zero lift, ft-lb
M_X	rolling moment, ft-lb
M_Z	yawing moment, ft-lb
C_L	lift coefficient, F_L/qS
C_D	drag coefficient, F_D/qS
T_c'	thrust coefficient, T/qS
C_Y	lateral-force coefficient, F_Y/qS
C_m	pitching-moment coefficient, M_Y/qSc_k
C_n	yawing-moment coefficient, M_Z/qSb
C_l	rolling-moment coefficient, M_X/qSb
ΔC_Y, ΔC_n, ΔC_l	incremental force and moments
Δg	incremental gravitational acceleration
$\frac{\partial C_m}{\partial C_L}$	slope of pitching-moment curve with lift coefficient

$$C_{Y_\beta} = \frac{\partial C_Y}{\partial \beta}, \text{ per deg}$$

$$C_{n_\beta} = \frac{\partial C_n}{\partial \beta}, \text{ per deg}$$

$C_{l_\beta} = \frac{\partial C_l}{\partial \beta}$, per deg

W	weight, lb
G	gearing ratio of control stick deflection to wing deflection
l	stick length, ft
g	acceleration of gravity, 32 ft/sec^2
C_{m_o}	pitching-moment coefficient at zero lift, M_{Y_o}/qSc_k

Subscripts:

k	keel
p	platform or wing pivot point

MODEL AND APPARATUS

The model used in the investigation consisted basically of a cargo platform attached to a parawing by means of an overhead truss arrangement. (See fig. 2.) The model was approximately 1/3.5 scale of the Ryan flexible-wing utility airplane except that, as pointed out in the "Introduction," no attempt was made to represent the flexibility characteristics of the airplane. The vehicle was powered by a pusher propeller located at the aft end of the platform and had a cockpit located at the front. The parawing used on the model was an existing configuration originally designed for other uses but was adapted to the model to expedite the flight tests. It was constructed of extremely lightweight materials without regard to specific structural standards. The leading-edge and keel members were made from 3/4-inch, thin-wall, aluminum tubing joined at the nose by an attachment formed by three thin leaf springs. A sweep angle of 50° was maintained by a spreader bar which was attached to the parawing leading edges and to the keel at approximately the 35-percent keel station. The fabric used to form the membrane of the parawing consisted of a nonporous Mylar film bonded to a nylon ripstop parachute cloth. The wing was supported by a pyramid-type structure mounted on the platform. The parawing was attached to the support structure by means of a universal joint so that it could be pitched or rolled with respect to the platform for control. Electrically operated servoactuators mounted on the platform were used to provide flicker type (full on or full off) deflections in pitch and roll in response to electrical signals generated by the pilots' control stick.

Power for the vehicle was supplied by a pneumatic motor driving a four-blade pusher propeller. The propeller blades were of 3-inch chord and were set at a blade angle of 14° measured at the 0.75 radius station. For some tests a rudder was mounted to the motor support structure directly behind the pusher propeller. A three-view drawing of the model is presented in figure 2 and photographs of the model and of the model servo-actuators and wing control assembly are presented in figures 3 and 4, respectively. Dimensional and mass characteristics of the model are presented in table I.

The investigation was conducted in the Langley full-scale tunnel. The static force tests were made with sting-type support equipment and strain-gage balances. The flight tests were made by using the technique and equipment illustrated in figure 5. Photographs of the model in flight are shown in figure 6 and a complete description of this flight-test technique is given in reference 4.

TESTS

Flight Tests

Flight tests were made to study the dynamic stability and control characteristics of the model over a keel angle-of-attack range from about 17° to 40° for light and heavy wing loading conditions. (See table I.) The model was flown by using the wing to provide longitudinal and lateral control and also with a rudder installed to supplement the lateral control in some tests. Flights were also made by using the rudder alone for lateral control. Wing roll angles used for lateral control varied from ±7° to ±15° and for all tests longitudinal control was provided by pitching the wing ±5°. Rudder deflections used in the flight tests varied from ±10° to ±20°

In the flight tests, longitudinal trim changes were achieved by shifting the center of gravity. Three different methods were used to accomplish these trim changes. One method consisted of rotating the wing with respect to the platform. Another consisted of sliding the wing along its keel axis so that the relative position of the wing with respect to the center of gravity was changed. In cases where trim could not easily be achieved by either of these two methods, a third method was used which consisted of adding lead weights to the front or rear of the platform. In most flights, longitudinal trim was obtained by the first method (since no provision was incorporated into the model for remotely sliding the wing with respect to the platform). The platform attachment point was located at the 0.42 keel station for most flights, although a few flights at high keel angles were made with the attachment point at the 0.50 keel station. In most cases, the center-of-gravity

positions presented in this paper are given in terms of nondimensional distances measured parallel and perpendicular to the parawing keel. With this nomenclature, the center-of-gravity range covered in the flight tests corresponded approximately to a vertical variation of 0.20 to 0.25 keel length and to a horizontal variation of 0.43 to 0.55 keel length.

Force Tests

For all the force tests, the strain-gage balance was mounted so that its longitudinal axis was alined with the cargo platform. The balance moment center was located at the reference center of gravity shown in figure 2. Since the forces and moments were therefore measured with respect to the platform angle, it was more convenient to use this angle rather than the keel angle as a reference for angle of attack. For this reason, the data are plotted in terms of platform angle and are discussed in terms of this angle except for a few cases where the data are referred to the keel angle for comparison purposes.

Power-off and power-on force tests were made to determine the static longitudinal and lateral stability and control characteristics of the model for use in correlation with the flight-test results. In the power-on longitudinal tests, effort was made in some cases to simulate steady level flight by trimming the model in both pitch and drag. Once the thrust setting of the motor was determined for these conditions, it was then held constant over the remainder of the angle-of-attack range.

In most of the power-off tests, the propeller was allowed to windmill; however, a few power-off tests were made with the propeller off for use in determining thrust coefficient. Most of the force tests were made over an angle-of-attack range of the platform from -10° to 20° for wing incidences of 10°, 20°, and 30°. (The angle-of-attack range of the keel covered by this group of tests varied from 0° to 50°.) Most of the lateral tests were made for sideslip angles of $\pm 5^\circ$ although a few tests were made over an angle-of-sideslip range from -20° to 20°. The tests to determine the lateral control effectiveness of the wing were made for a range of wing roll angles of 5°, 10°, and 15° and tests to determine the rudder control effectiveness were made for rudder deflections of $\pm 10^\circ$ and $\pm 20^\circ$.

All the tests were run at a dynamic pressure of about 1.20 pounds per square foot which corresponds to an airspeed of about 42 feet per second at standard sea-level conditions and to a test Reynolds number of about 2,140,000 based on the parawing keel length of 8.0 feet.

RESULTS AND DISCUSSION

Force Tests

Static longitudinal stability and trim.- Since the force-test results are presented mostly in terms of platform angle, any reference to angle of attack in this section means platform rather than keel angle of attack unless otherwise noted.

The results of force tests to determine the static longitudinal stability and trim characteristics of the model are presented in figure 7 for wing incidences of 10°, 20°, and 30°. These data show that the effect of power on the longitudinal characteristics of the model was relatively small except for the $i_w = 30°$ condition where some consistent changes in lift coefficient occurred with changes in power. For this condition, increasing power reduced the lift coefficient at a given angle of attack but delayed the stall and increased the maximum lift coefficient. These effects of power are probably related to the close proximity of the parawing trailing edge to the propeller slipstream for the $i_w = 30°$ condition.

In order to permit a better comparison of the effects of changes in wing incidence on the longitudinal characteristics of the model, the data of figure 7 for i_w conditions of 10°, 20°, and 30° are replotted in figure 8 for the power-off case. Also presented in figure 8(a) are data for the model with the parawing off. The data for the complete configuration show, as expected, that increasing the angle of incidence of the parawing increased the lift coefficient at which pitch trim occurred and reduced the static longitudinal stability. At angles of attack near the stall, the static longitudinal stability of the model increased rather sharply for the angles of incidences investigated. Although all the conditions showed maximum values of L/D of about 4.5, only the $i_w = 20°$ condition was trimmed at the angle of attack where the maximum value of L/D occurred. The data for the model with the parawing off of figure 8(a) show relatively small values of lift, drag, and pitching-moment characteristics.

Although the center-of-gravity reference for all the force tests was held fixed with respect to the platform (see fig. 2), this reference changed considerably in terms of distances parallel and perpendicular to the parawing keel when the angle between the keel and platform was changed. In order to illustrate this point and to show the relationship between the center-of-gravity location and static longitudinal stability and trim, the center-of-gravity locations corresponding to the i_w conditions of 10°, 20°, and 30° are plotted in terms of x_k/c_k

and z_k/c_k in figure 9. Also presented in figure 9 are lines representing center-of-gravity locations for constant stability and trim at constant lift coefficient which were derived by using simple moment transfer equations and the power-off force-test data from figure 8. These equations were used to calculate values of x_k/c_k and z_k/c_k which would give constant values of $C_m = 0$ and $\frac{\partial C_m}{\partial C_L} = 0$, -0.05, and -0.10 for given lift coefficients. The calculated results are based on linear data and are therefore not directly applicable to high angle-of-attack conditions where wing stall produces large nonlinear variations in the aerodynamic data. This figure is similar to that developed in reference 3 and is useful in determining approximate stability and trim information very readily. From this information, the approximate regions of x_k/c_k and z_k/c_k in which the center of gravity must be located to produce both stability and trim are easily determined.

Static lateral stability characteristics.- Representative static lateral characteristics of the model measured over an angle-of-sideslip range from -20° to 20° are presented in figures 10(a), 10(b), and 10(c) for i_w conditions of 10°, 20°, and 30°, respectively. These data show a fairly linear variation of the lateral coefficients C_Y, C_n, and C_l with sideslip angle and show that the effects of power are generally small except for lateral trim changes. These trim changes are probably associated with torque and with incremental side forces and yawing moments introduced by asymmetrical flow conditions resulting from slipstream rotation.

The static lateral stability parameters C_{Y_β}, C_{n_β}, and C_{l_β} determined from figure 10 at sideslip angles of ±5° and from other lateral tests made at ±5° are presented in figure 11. These data show that the model was statically directionally stable and had positive dihedral effect for the angle-of-attack range investigated. The data of figures 11(b) and 11(c) show that the rudder generally increased the directional stability and positive dihedral effect of the model.

In order to permit a direct comparison of the effects of changes in i_w on the lateral characteristics of the model, the data of figure 11 for i_w conditions of 10°, 20°, and 30° are replotted in figure 12 for the power-off case. This comparison is made for the power-off case since the effects of power are relatively small. The data of figure 12 were transferred to the stability axes and replotted in figure 13 for use in making an analysis which is presented later in the report. The data of figures 12 and 13 show that increasing the angle of incidence of the parawing produced no consistent effect on directional stability but generally increased the positive dihedral effect

at a given platform angle except for the $i_w = 30^\circ$ condition where wing stall occurred at the higher angles of attack.

Static lateral control characteristics.- The static lateral control characteristics produced by rolling the parawing with respect to the platform are presented in figure 14 for i_w conditions of 10°, 20°, and 30° and are summarized in figures 15 and 16 for the power-off case. The data for the i_w conditions of 20° and 30° (figs. 14(b) and 14(c)) show that rolling the wing produced favorable rolling moments but also gave fairly large values of adverse yawing moments at high angles of attack. Power effects were generally negligible except for the $i_w = 30^\circ$ condition where power reduced the lateral forces and moments produced by the rolled wing over the entire angle-of-attack range. The data of figure 16 show that the adverse yawing moments and favorable rolling moments produced by rolling the wing generally increased with an increase in i_w.

Analysis of the data to determine the source of the yawing moment produced by rolling the wing indicates that there are three factors involved, one adverse and two favorable. The adverse yawing moments at high angles of attack appear to result primarily from the fact that, when the wing is rolled, the lift vector tilts and therefore has a lateral component. This lateral component is approximately equal to $C_L \sin \phi$ and, since it is aft of the center of gravity, produces an increment of adverse yawing moment. This increment of the adverse yawing moment at high angles of attack is reduced considerably, however, by the two favorable factors involved. These factors are the drag of the wing and the directional stability parameter C_{n_β}. The drag produces a favorable yawing moment because this force is located above the pivot point and is therefore displaced laterally when the wing is rolled. The C_{n_β} parameter becomes significant in this case because rolling the wing introduces an angle of sideslip. Since the wing is directionally stable, the sideslip angle introduced by rolling the wing produces an increment of favorable yawing moment.

In order to determine how reliably the above factors could be used in computing the adverse yawing moments produced by rolling the wing, incremental yawing moments based on these factors were calculated for comparison with the measured data. In addition, calculations were made to determine the side-force and rolling-moment increments produced by rolling the wing. The side-force increments were computed by assuming that the only two factors involved were $C_L \sin \phi$ and $C_{Y_\beta}(\beta)$ where β equals $\alpha_K \sin \phi$. The rolling-moment increments were computed by assuming that $C_L \sin \phi$ multiplied by the vertical distance from this vector to the center of gravity was one factor and the other was $\left(C_{l_\beta}\right)(\beta)$.

These results, together with measured data for the $i_w = 20^\circ$ condition from figure 16, are presented in figure 17. The data of figure 17 show that the calculated and measured data are generally in fairly good agreement for the yawing-moment and rolling-moment cases, but the side-force results are in poor agreement.

In the analysis of the lateral control data, it became apparent that the data of figure 16 are not presented in the most convenient form for use in direct correlation with flight-test results for steady level-flight conditions. For instance, in steady level flight, where the lift is equal to the weight and therefore does not vary with angle of attack, it is obvious that these effects are not a true indication of the control effectiveness of the wing. In order to obtain control data which were more representative of these conditions, the incremental forces and moments of figure 16 were divided by lift coefficient and are presented in figure 18.

The data of figure 18 are referred to as lateral control effectiveness parameters and, although the magnitude of these results is not significant (except possibly to represent some equivalent moment arm), the variations in these parameters with angle of attack are believed to be representative of those likely to be experienced in flight with a configuration of this type. It is interesting to note that these data indicate a decrease in the rolling effectiveness of the wing with increasing angle of attack (except for the $i_w = 10^\circ$ condition where the parawing was unloaded) and adverse yawing moments in the positive angle-of-attack range which increase with increasing angle of attack.

The results of tests to determine the lateral control effectiveness of the rudder are presented in figure 19. These data show that incremental yawing moments produced by the rudder were small in the power-off case but, as would be expected, were relatively large for the power-on condition.

Flight Tests

The model behavior during flight was observed by the pitch pilot located at the side of the test section and by the roll-yaw pilot located at the rear of the test section. The results obtained in the flight tests were primarily in the form of qualitative ratings of flight behavior based on pilot opinion. Motion-picture records obtained in the tests were used to verify and correlate the ratings for the different flight conditions. A motion-picture film supplement covering the flight tests of the model has been prepared and is available on loan. A request card form and a description of the film are found at the back of this report on the page immediately preceding the abstract and index page.

In model flight-test studies, there are several factors which must be considered in order to interpret correctly the results in terms of full-scale configurations. In addition to the normal scale effects, there are additional factors such as cable drag, flexibility, and stick forces which should be considered for the present model. The effects of the flight cable depend on the relative sizes of the model and cable and vary from small trim changes to considerable stability and control changes. The effects of the flight cable in this case (discussed in more detail in a later section) were relatively small because of the large size of the model in comparison with the size of the cable.

As mentioned previously, parawing configurations are subject to flexibility characteristics which may introduce large discrepancies in aerodynamic data. No attempt was made to determine the effects of flexibility on the present model but these effects are believed to be relatively large in this case because considerable deformation of the parawing members with loading were noted in the tests. For this reason, caution should be used in applying the data directly to other parawing configurations having different flexibility characteristics.

Another factor which would have great significance in the control evaluation for full-scale parawing vehicles (but which was not considered in the model tests) is that of stick forces. The analysis (see appendix) has indicated that for the control system used on the model (pitching the wing for longitudinal control and rolling the wing for lateral control), it was possible for these forces to become objectionably large for a full-scale vehicle of this type.

All reference to angle of attack in the discussion of flight-test results means angle of attack of the keel rather than angle of attack of the platform.

Longitudinal stability and control characteristics.- In a configuration such as that of the present investigation in which center-of-gravity changes are used to produce longitudinal trim and control, it is especially important to have the test center-of-gravity range well defined. For this reason, the range of center-of-gravity positions used in the flight tests are presented in figure 20(a) with reference to the model platform and in figure 20(b) with reference to the keel. For correlation purposes, the center-of-gravity positions and lines of constant stability of figure 9 are also presented in figure 20(b). From this figure, it is possible to estimate the range of values of static longitudinal stability covered in the flight tests. This range appears to vary from approximately zero to 11 percent. It should be emphasized, however, that the constant stability lines shown in figure 20(b) were constructed by assuming that the aerodynamic center did not vary with lift coefficient. This assumption is valid except near the stall where a rearward shift in the aerodynamic center resulted in a sharp increase in static

longitudinal stability. (See fig. 8.) This condition means that static longitudinal instability was approached but probably never experienced in the flight tests.

As mentioned previously, longitudinal trim was obtained in most cases by rotating the platform with respect to the wing or by adding weights to the front or rear of the platform. In the flight tests it was found that for a given angle of attack the platform angle of attack required for trim of the keel was higher than those indicated by force-test results. This difference is believed to be associated primarily with flight cable drag which introduced incremental positive pitching moments to the model. In order to trim out these additional moments, the platform had to be rotated further forward with respect to the wing. There did not appear, however, to be an appreciable effect of platform angle on the longitudinal flight characteristics of the model based on tests in which several platform angles were used to fly constant keel-angle conditions.

The dynamic longitudinal stability and trim characteristics of the model were found to be satisfactory over the angle-of-attack range investigated (keel angles of 17° to 40°) for both the light loading and heavy loading conditions. The decrease in static longitudinal stability of the model as the trim lift coefficient increased (below the stall) did not appear to be of great significance in the flight behavior of the model except possibly at moderately high lift coefficients. In this region there was some indication that the model was not as steady longitudinally as it was at the lower lift coefficients although there was never any indication of static longitudinal instability and flights attempted near the stall were usually terminated by a stable, pitch-down motion. In the light loading condition some difficulty was experienced at times in establishing trim conditions because of the offset of the center of gravity above the thrust axis. This effect was particularly noticeable at the higher angles of attack where power effects were more pronounced. With the heavier loadings, the center of gravity was either on or below the thrust axis and much less difficulty was experienced in establishing and maintaining trim conditions. In the heavier condition, the model was somewhat less responsive to control or gust disturbances and for this reason was probably a little steadier longitudinally than for the light condition. For both the light and heavy conditions, however, the model was generally easy to fly and once trim conditions were established, smooth flights of considerable duration were achieved in which little corrective control was required.

Pitching the wing to provide longitudinal control provided a satisfactory means of controlling the model. In the flight tests, it was observed that there was an immediate rotation of the platform rather than of the wing in response to a control signal for the model in the light condition. To the pitch pilot, the wing appeared to remain essentially stationary while the platform rotated either backward or forward

as control was applied. This effect was also apparent for heavy loading conditions although at times there appeared to be some initial wing rotation in response to control in this case.

Lateral stability and control characteristics.- The lateral stability characteristics of the model were found to be generally satisfactory over the angle-of-attack range of the tests. The model was directionally stable and the lateral oscillations were well damped for both the light and heavy wing loading conditions.

Rolling the wing for lateral control provided a satisfactory means of controlling the model in the lower angle-of-attack range (17° to 25°), but this control became progressively weaker with increasing angle of attack. Up to an angle of attack of about 25°, the model responded quickly to control and very little attention was required by the lateral control pilot to maintain smooth flight. To the lateral control pilot, the wing appeared to remain essentially stationary in roll while the platform rotated from side to side as control was applied. This effect was especially true for the light loading condition but, as the loading was increased, some initial wing response to a control was also observed.

As the angle of attack of the keel increased beyond about 25°, the control provided by the wing became progressively weaker until at angles of about 35° this type of control appeared to be ineffective. It was extremely difficult to keep the model under control and positioned in the test section in the high-angle-of-attack range because the initial response of the model to roll control was opposite to that desired. This loss in control effectiveness is probably associated with the decrease in rolling effectiveness of the wing with increasing angle of attack and the adverse yawing moments associated with this type of control (see fig. 16) in combination with the large values of positive effective dihedral at high angles of attack. The model recovered very slowly from a disturbance and, even though the pilot applied constant attention to the controls, sustained flights could not be made above an angle of attack of about 35°.

In the preceding section, it was pointed out that the drag of the flight cable introduced incremental positive pitching moments which required higher platform angles of attack for trim. Since such an effect resulted in a more forward center-of-gravity location and therefore an increase in moment arm from the center of gravity to the lift vector of the wing, it would appear that the adverse yawing moments produced by rolling the wing might be large in this case. Analysis (similar to that used in the discussion of the force-test results) indicated, however, that this effect was only of the order of about 10 percent and therefore did not appreciably affect the control characteristics of the model in the tunnel flight tests.

In order to provide a source of favorable yawing moments in the high-angle-of-attack range, a rudder surface was installed on the model directly behind the pusher propeller. When the rudder was coordinated with the wing control, the model had satisfactory lateral control characteristics at keel angles of attack up to 40° (highest angle flown). In fact, because of the high values of effective dihedral at these higher angles of attack, the model could be flown satisfactorily with the rudder alone. The response of the model to rudder control was found to decrease as the angle of attack was reduced. In the angle-of-attack range from 25° to 30°, the response to rudder control was about equal to that provided by the wing control and the model could be flown equally well with either type of control. The lateral response of the model to rudder control became so poor at angles of attack near 20° that it became impossible to make sustained flights with rudder alone. This decrease in response of the model to rudder control was apparently primarily a result of the decrease in positive effective dihedral of the model as the angle of attack was reduced. (See figs. 12 and 13.)

SUMMARY OF RESULTS

The results of the investigation to determine the flight characteristics of the model of a parawing utility vehicle may be summarized as follows. Although stick forces or the effects of flexibility were not taken into account in the investigation (and this fact may limit the usefulness of the results as far as direct application to other parawing configurations is concerned), it is believed that the results do provide a qualitative indication of the overall flight characteristics of a configuration of this type.

1. The model had satisfactory longitudinal and lateral stability characteristics over the angle-of-attack range investigated (keel angles of 17° to 40°).

2. The control system used on the model (pitching and rolling the wing) proved to be generally satisfactory except for lateral control at high angles of attack. The lateral control provided by rolling the wing was satisfactory in the lower angle-of-attack range investigated (keel angles of 17° to 25°), but this control became progressively weaker with a further increase in angle of attack (because of a decrease in rolling effectiveness of the wing and large adverse yawing moments associated with this type of control in combination with large values of positive dihedral effect) until at angles of attack above about 35° it appeared to be ineffective.

3. The model could be flown satisfactorily up to keel angles of attack of 40° (highest angle flown) with a rudder surface installed

directly behind the pusher propeller and coordinated with the wing control. Because of the high effective dihedral in the high-angle-of-attack range, satisfactory flights could also be made by using the rudder alone for control.

Langley Research Center,
National Aeronautics and Space Administration,
Langley Air Force Base, Va., February 13, 1962.

APPENDIX

ESTIMATIONS OF HINGE-MOMENT AND STICK-FORCE CHARACTERISTICS OF A PARAWING UTILITY VEHICLE

Because of the unusual nature of the parawing utility vehicle investigated, it appeared advisable to give some attention to the hinge-moment and stick-force characteristics involved in a configuration of this type. Since it was possible to obtain some preliminary information based on the force-test data presented, a few simple calculations were made to determine stick-force characteristics by using some assumed full-scale dimensional and mass characteristics. A brief analysis of these calculated results is presented in the following paragraphs.

Longitudinal Characteristics

In order to obtain some indication of the longitudinal stick forces involved, calculations were made in which it was assumed that the longitudinal stick force required for trim could be represented by the following equation:

$$\text{Stick force} = \frac{(C_m)_p q S c_k}{G l} \tag{1}$$

where $(C_m)_p$ is the pitching-moment coefficient about the wing pivot point (and therefore is equivalent to the hinge moment of the wing about this point) and G and l are the longitudinal gearing ratio and stick length, respectively. If $(C_m)_p$ is replaced by $\left(C_{m_o} + \frac{\partial C_m}{\partial C_L} C_L\right)_p$ and W/SC_L is substituted for q, equation (1) then becomes

$$\text{Stick force} = \left(\frac{C_{m_o}}{C_L} + \frac{\partial C_m}{\partial C_L}\right)_p \frac{W c_k}{G l} \tag{2}$$

From equation (2) it is apparent that $\left(C_{m_o}\right)_p$ determines the stick-force gradient with speed and therefore the stick force per g relationship in a configuration of this type. In order to show more clearly the effects of these parameters on stick-force characteristics

(without getting into nonlinearities of measured force-test data which sometimes obscure significant points), calculations were made in which it was assumed that the hinge-moment variation with lift coefficient was linear and that C_{m_o} was 0.02 in one case and -0.02 in another. These calculations were made by using the following mass and dimensional characteristics:

W, lb	1,500
S, sq ft	550
c_k, ft	28
G	3
l, ft	2.25

The results of these calculations are presented in figure 21(a). The assumed hinge-moment data shown at the top of this figure are representative of the variation of hinge moment with lift coefficient for three different parawing pivot-point locations. These data are presented in this manner since in this configuration there are no elevators or trim tabs and the only means of changing these hinge-moment variations is by changing the parawing pivot-point location. The results of figure 21(a) show that, for a positive value of C_{m_o}, a stable stick-force gradient with speed and positive stick force per g are obtained, whereas, for a negative value of C_{m_o}, the opposite trends occurred. From these results and from equation (2), which shows that the stick-force gradient and the stick force per g relationship vary directly with C_{m_o}, it is evident that a small, positive value of C_{m_o} is necessary in order to insure the most desirable stick-force characteristics.

With the significant points of the above discussion in mind, calculations similar to those presented were repeated with the exception that measured pitching-moment data for the parawing alone condition were used instead of the assumed values of the previous case. These data (obtained from fig. 8 for $i_w = 20^\circ$ and $T_c' = 0$ by transferring the pitching moments from the center of gravity to the pivot point) together with the calculated stick forces are presented in figure 21(b). The pitching-moment data of this figure are fairly linear up to a lift coefficient of about 0.8 and indicate very small values of C_{m_o}. Within this lift-coefficient range (corresponding to a speed range of approximately 35 to 65 knots), the calculations show a stable stick-force gradient and stick forces required for trim of the order of 50 pounds or less for a pivot-point location of 0.465 keel length. At higher lift coefficients, the stick forces become very large because of the large increases in the slopes of the pitching-moment curves beyond this point. It should

be emphasized that unpublished force-test results of several parawing configurations have shown that C_{m_o} varied considerably from one parawing to another. These differences in C_{m_o} could possibly be attributed to small differences in material, construction, or deformation of the parawing fabric, keel, or leading-edge members with loading. Because of the difficulty of evaluating such factors with any degree of accuracy from one case to another, it appears that predictions of hinge-moment and stick-force characteristics for large-scale parawing configurations based on small model tests could be misleading and that caution should be used in applying such information to parawing configurations in general.

Lateral Characteristics

In order to obtain some preliminary information pertaining to the lateral stick forces involved in a parawing configuration such as that of the present investigation, stick-force calculations based on the lateral-control data presented in figure 15 were made. It was assumed that the lateral stick force required for trim could be approximated by the following equation:

$$\text{Stick force} = \frac{\left(C_l\right)_p qSb}{Gl} \tag{3}$$

where in this case $\left(C_l\right)_p$ is the rolling-moment coefficient about the parawing pivot point and represents the moment which must be trimmed out by the pilot. The value of $\left(C_l\right)_p$ for these calculations was determined from figure 15 for $i_w = 20^\circ$ and $T_c' = 0$ by transferring the rolling moments from the center of gravity to the pivot point. The other factors used in these calculations were the same as those used to calculate the longitudinal stick forces. The rolling-moment coefficient data (presented for a wing roll angle of 15°) and calculated stick forces are presented in figure 21(c). These data show that the rolling moments about the pivot point increased rapidly with increasing lift coefficient with the result that near the stall (approximately 30 knots airspeed) the lateral stick forces required for trim increased up to values of about 200 pounds.

REFERENCES

1. Rogallo, Francis M., Lowry, John G., Croom, Delwin R., and Taylor, Robert T.: Preliminary Investigation of a Paraglider. NASA TN D-443, 1960.

2. Naeseth, Rodger L.: An Exploratory Study of a Parawing as a High-Lift Device for Aircraft. NASA TN D-629, 1960.

3. Hewes, Donald E.: Free-Flight Investigation of Radio-Controlled Models With Parawings. NASA TN D-927, 1961.

4. Paulson, John W., and Shanks, Robert E.: Investigation of Low-Subsonic Flight Characteristics of a Model of a Hypersonic Boost-Glide Configuration Having a 78° Delta Wing. NASA TN D-894, 1961.

TABLE I.- MASS AND DIMENSIONAL CHARACTERISTICS OF THE MODEL

Weight, lb:	
Light condition	31.00
Heavy condition	53.03
Wing loading, lb/sq ft:	
Light condition	0.685
Heavy condition	1.17
Moment of inertia (light condition), slug-ft^2:	
I_X	2.65
I_Y	4.27
I_Z	2.04
Parawing dimensions:	
Area (developed, 45° leading-edge sweep), sq ft	45.30
Span (based on 45° leading-edge sweep condition), ft	11.32
Keel length, ft	8.0
Rudder dimensions:	
Area, sq ft	0.834
Span, ft	1.43
Chord, ft	0.584
Aspect ratio	2.45

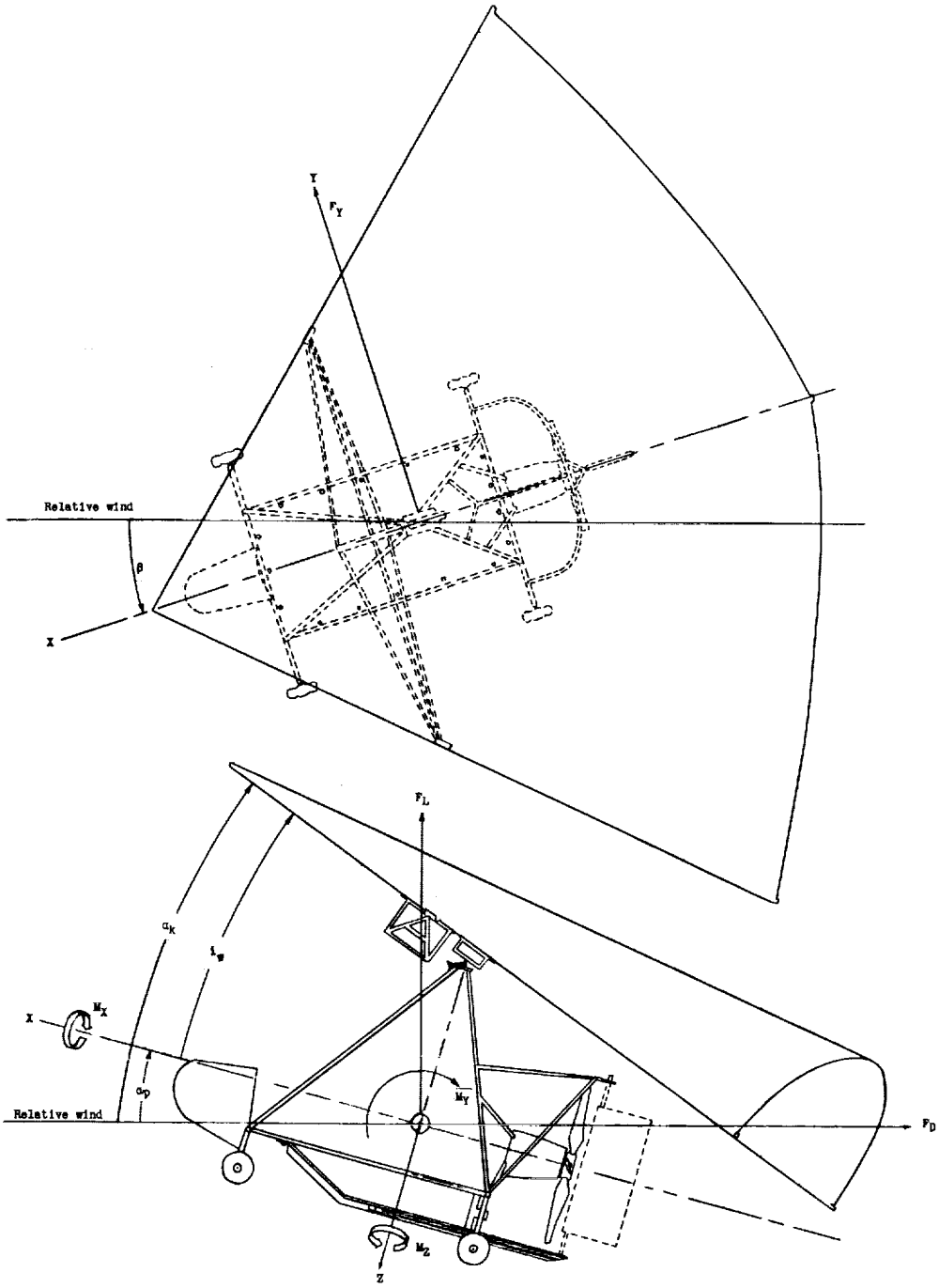

Figure 1.- System of axes used in the investigation. The longitudinal data are referred to wind axes and the lateral data are referred to body axes unless otherwise specified. Arrows indicate positive direction of moments, forces, and angles.

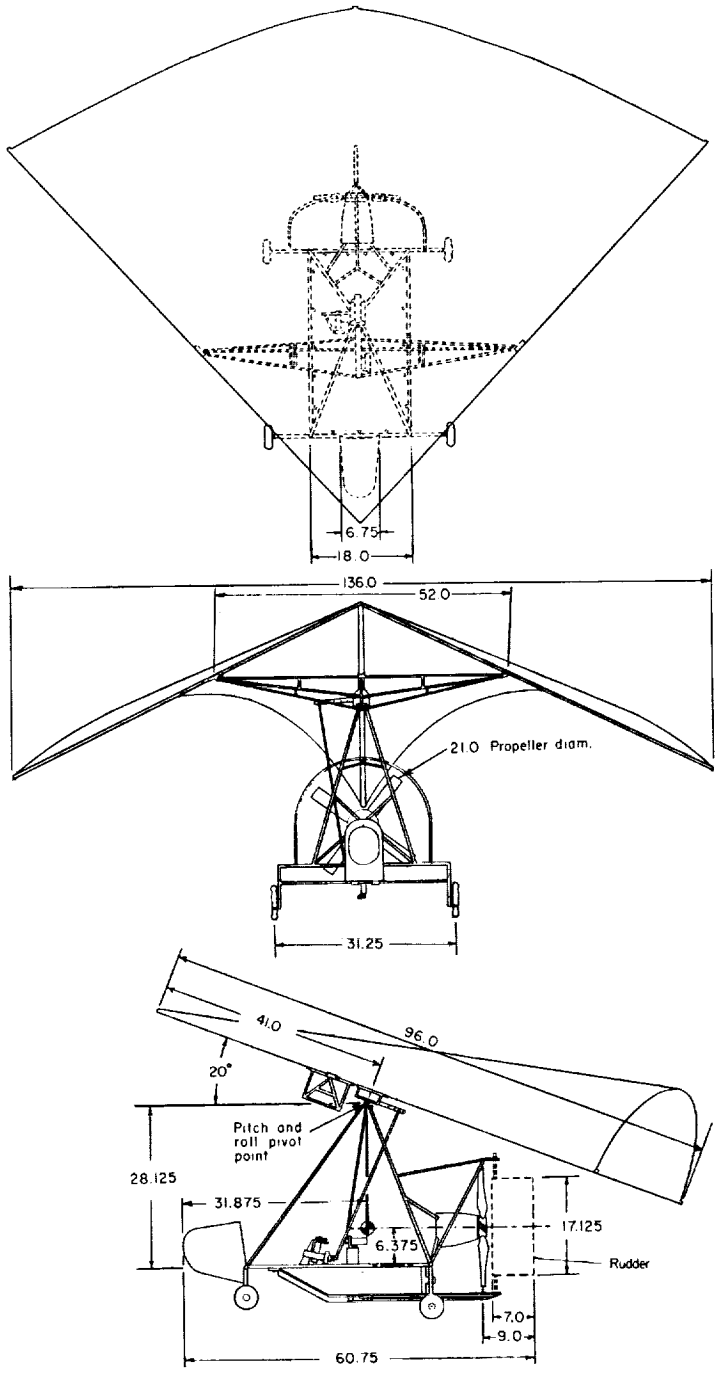

Figure 2.- Three-view drawing of model used in the investigation. All dimensions are in inches.

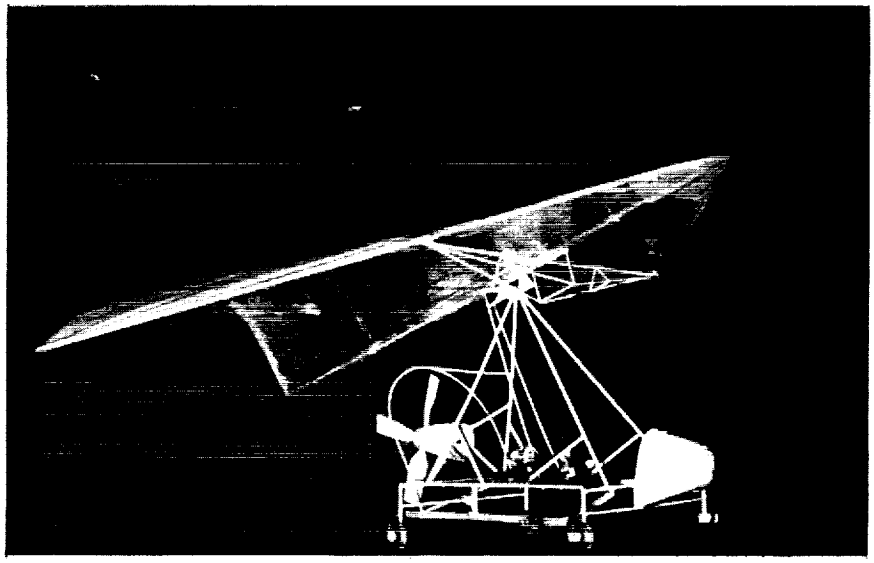

L-61-1126

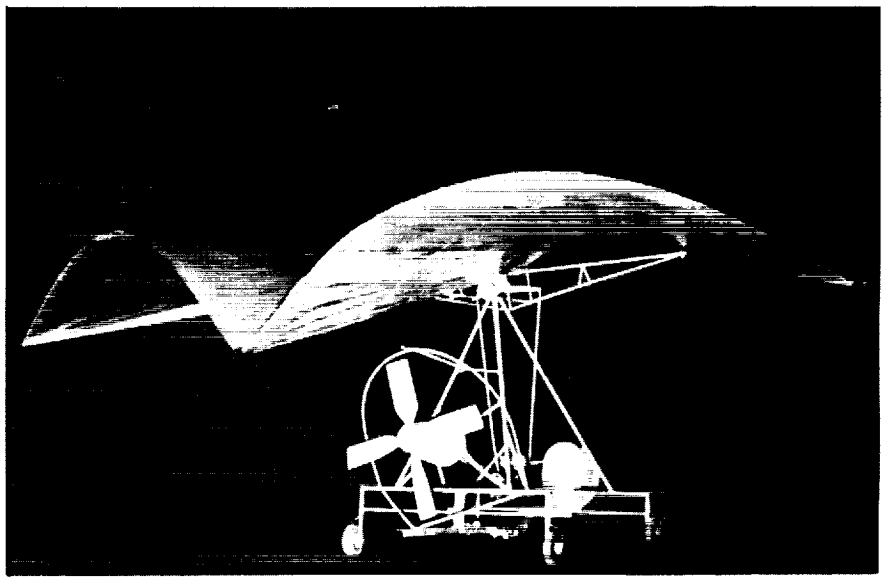

L-61-1127

Figure 3.- Photographs of model used in the investigation.

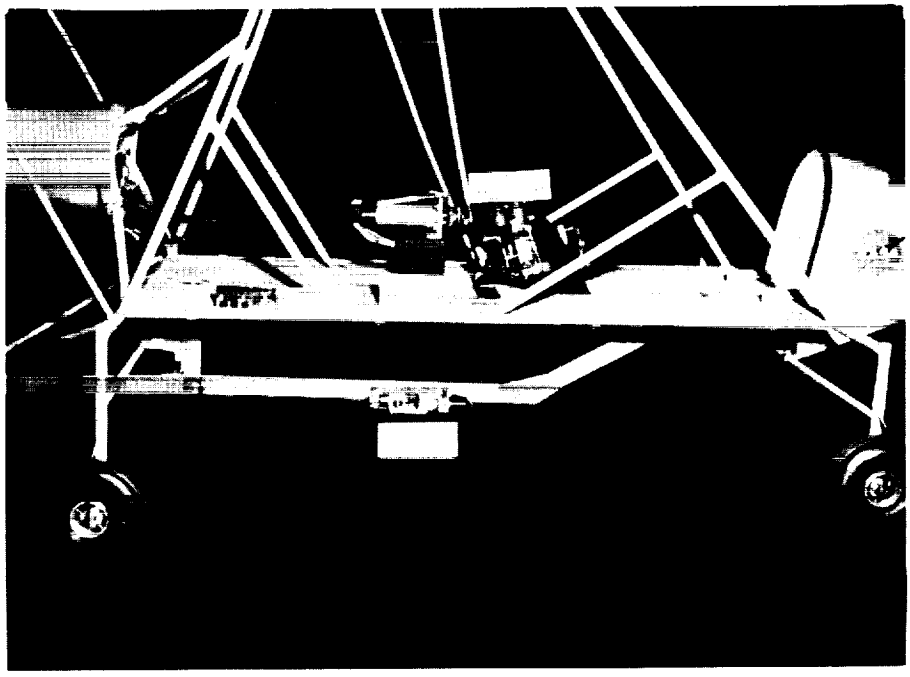

L-61-1113

Figure 4.- Photograph of model showing control mechanisms used in the investigation.

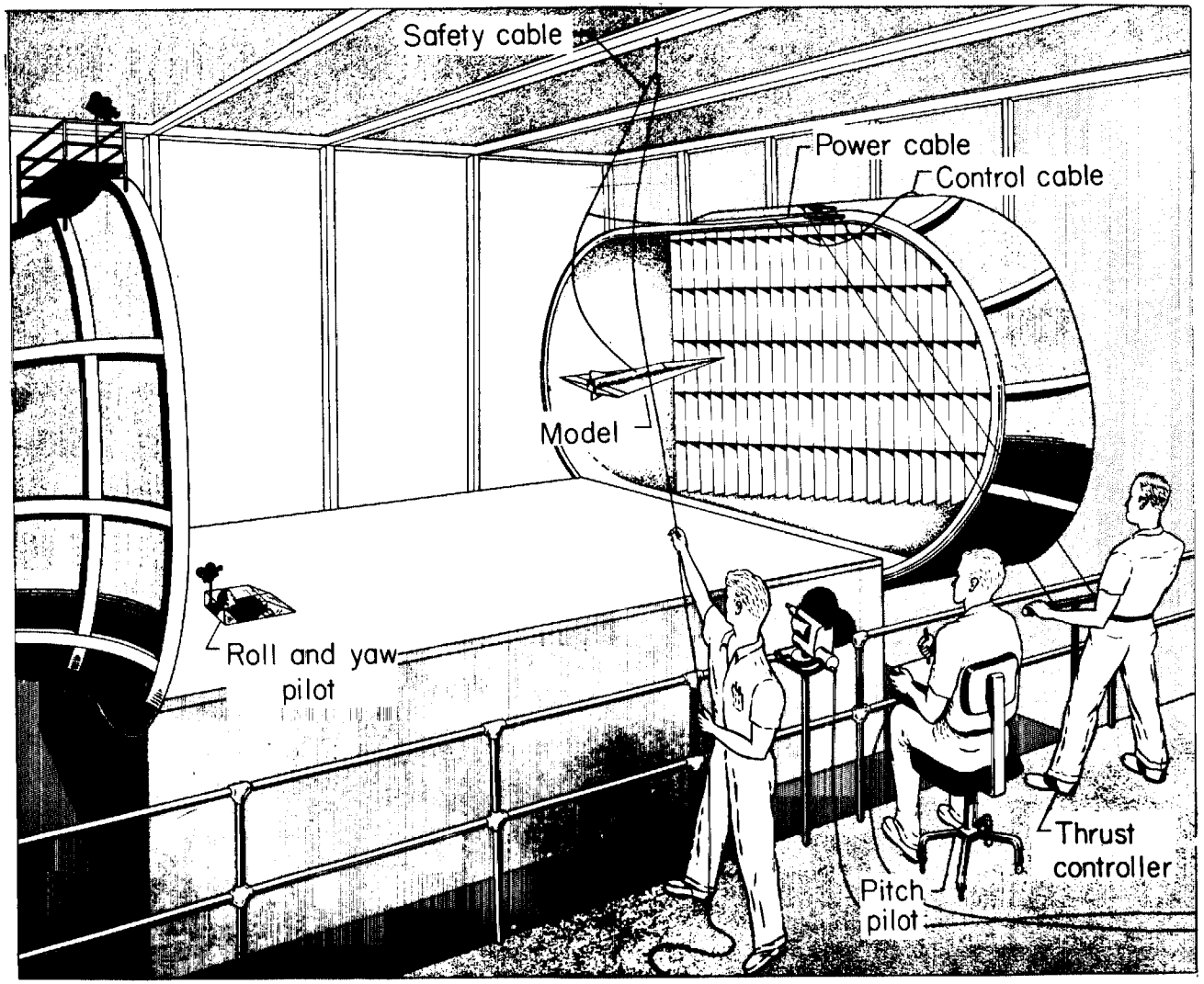

L-62-580

Figure 5.- Sketch of flight-test setup in the Langley full-scale tunnel.

L-61-424

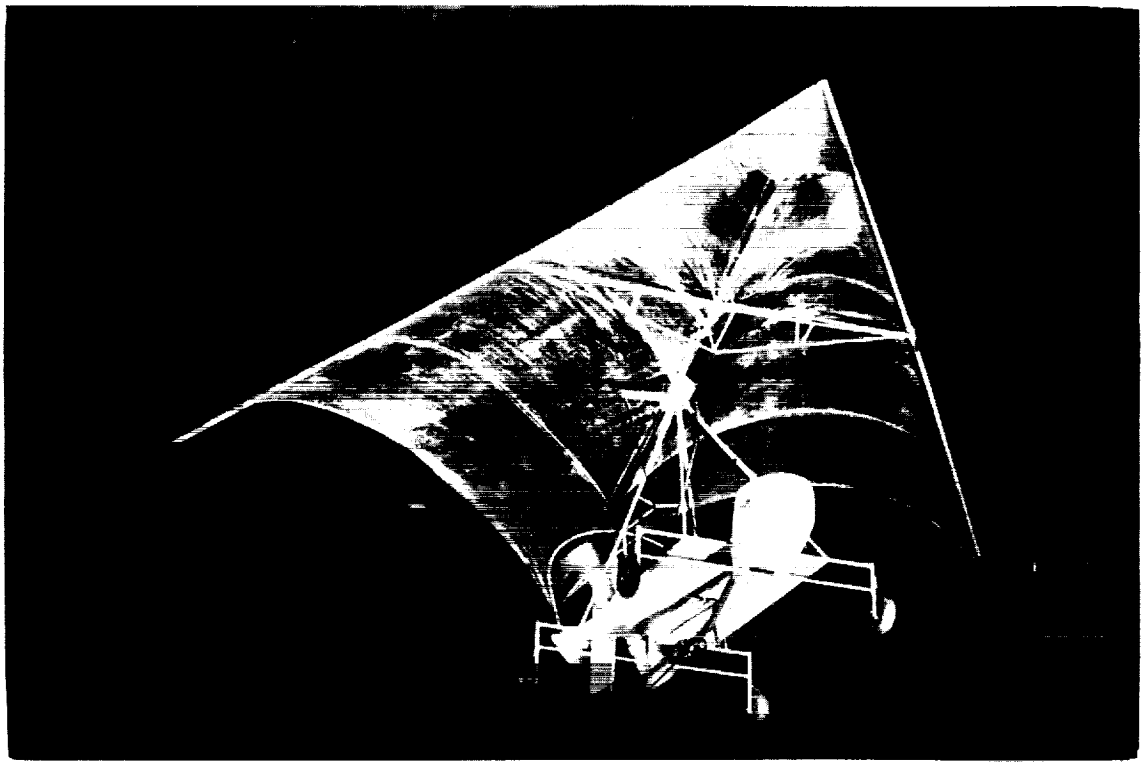

L-61-426

Figure 6.- Photographs of model flying in the Langley full-scale tunnel.

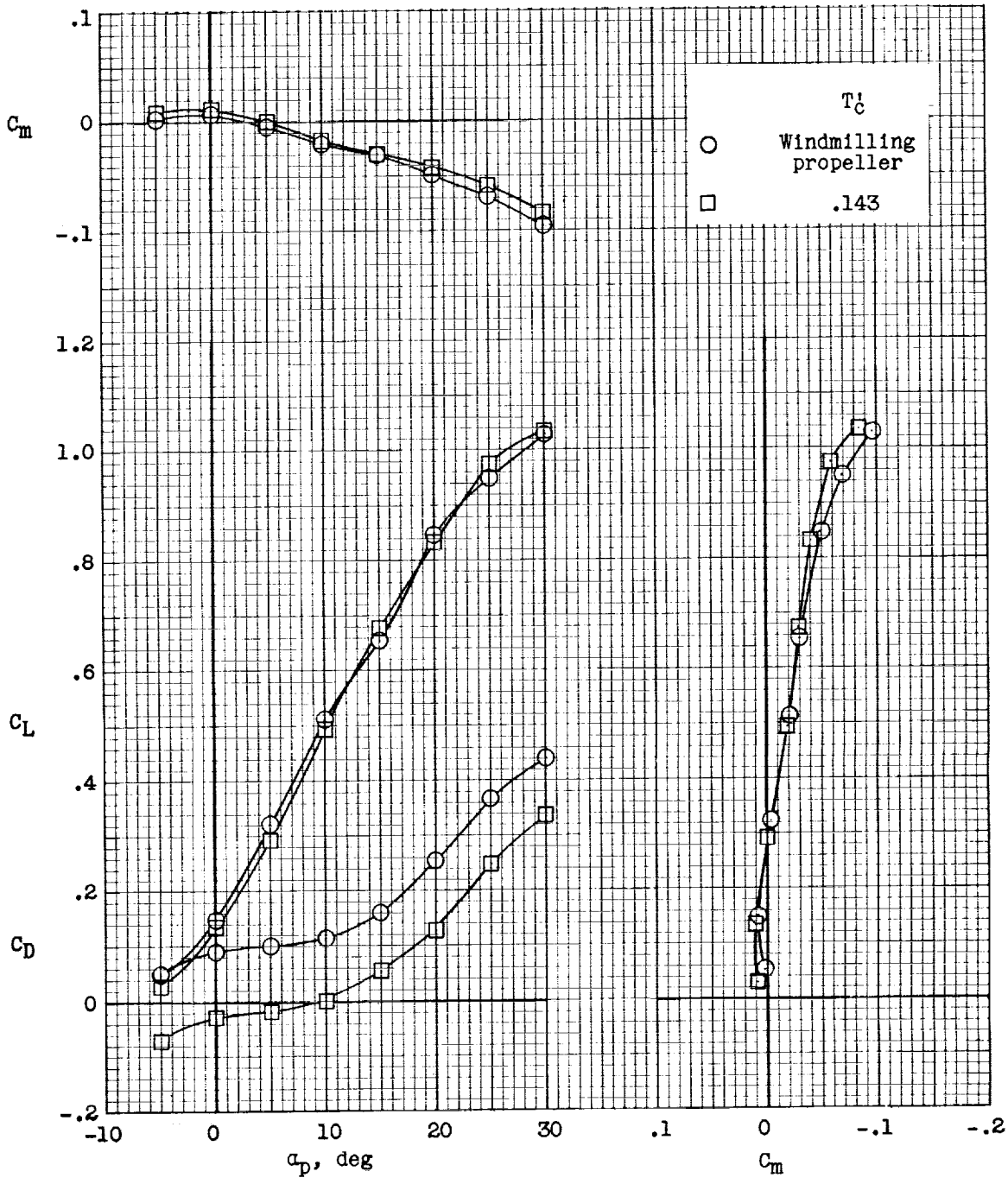

(a) $i_w = 10^o$.

Figure 7.- Static longitudinal characteristics of the model.

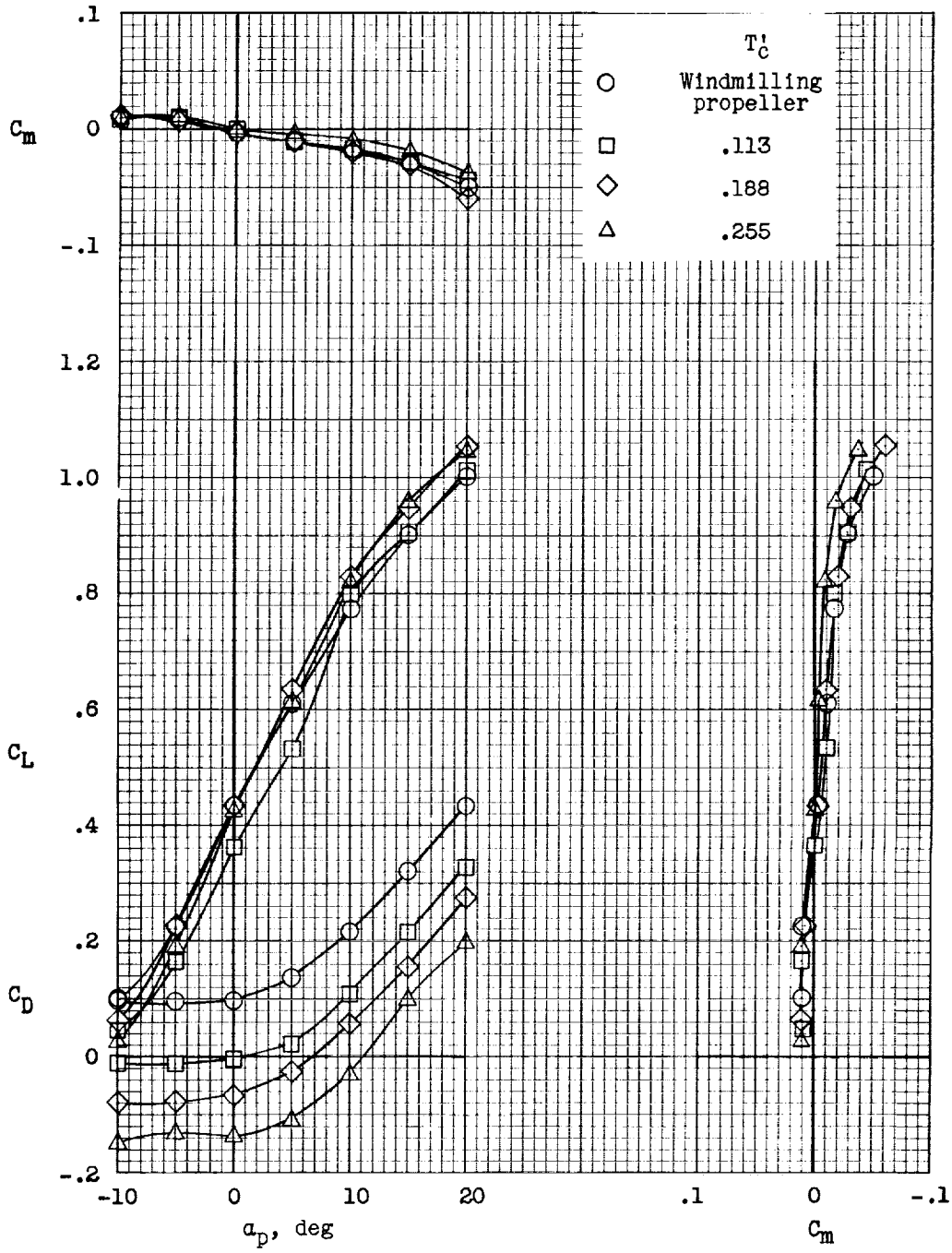

(b) $i_w = 20^\circ$.

Figure 7.- Continued.

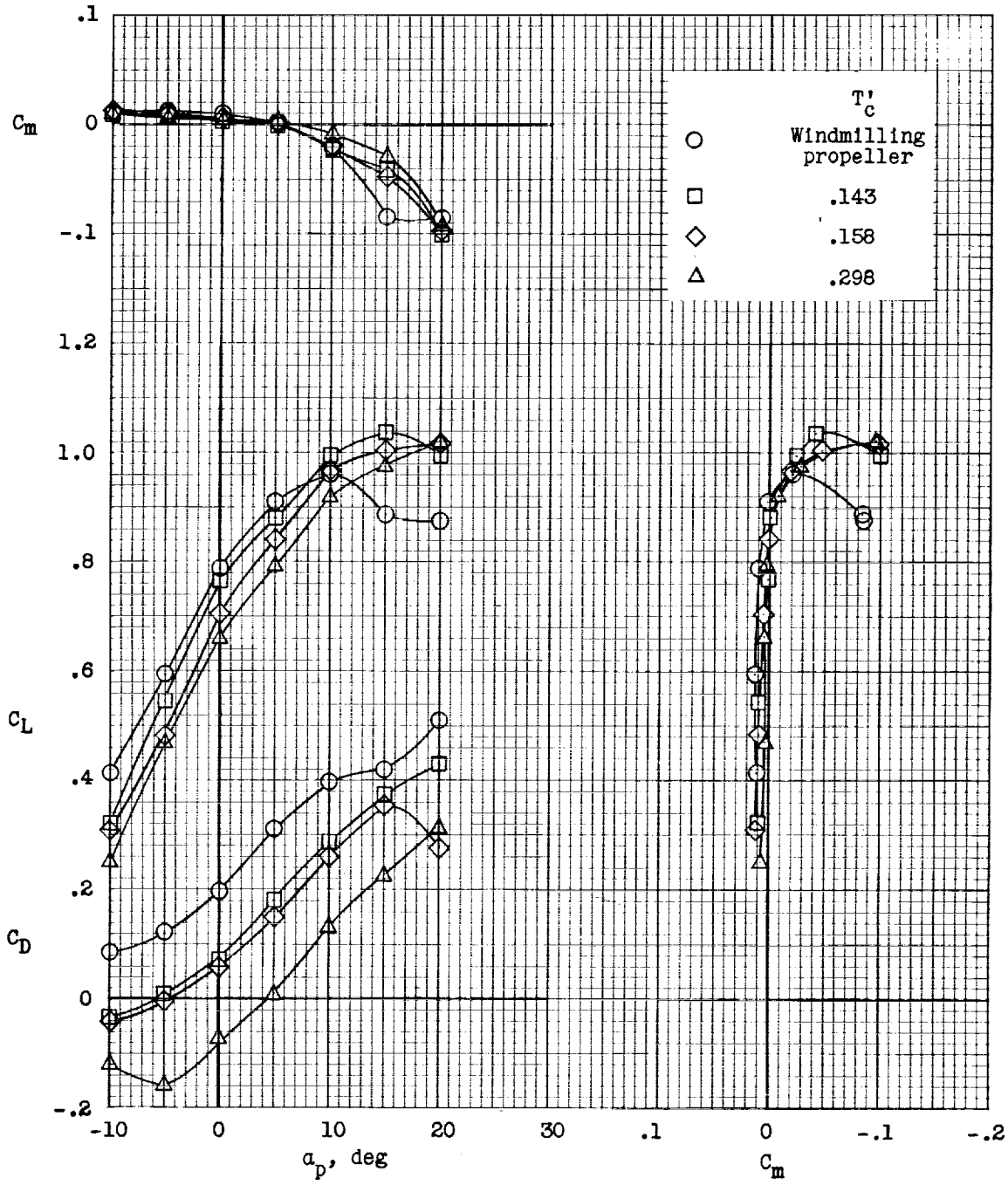

(c) $i_w = 30^\circ$.

Figure 7.- Concluded.

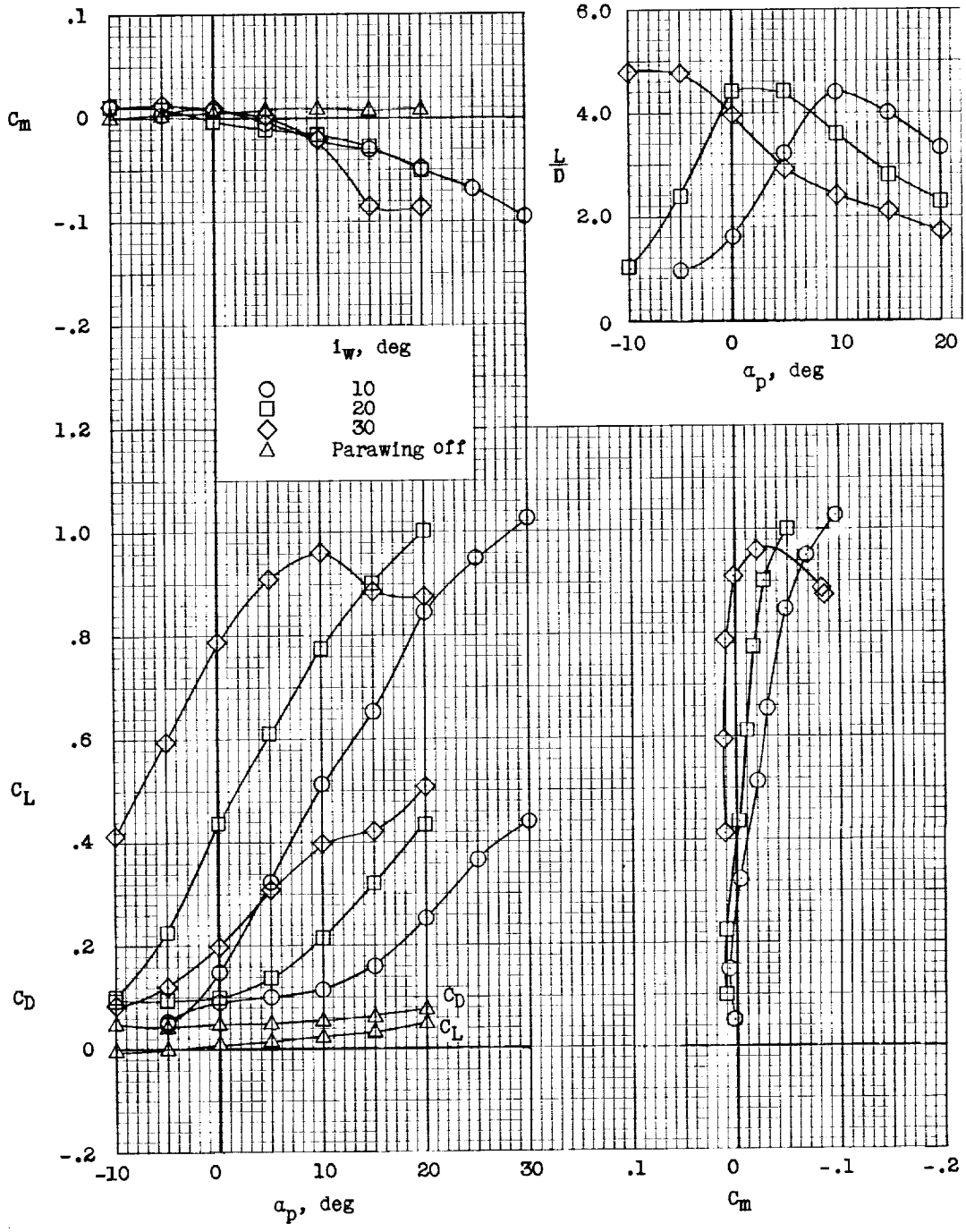

(a) Data plotted against platform angle.

Figure 8.- Comparison of static longitudinal characteristics of the model. Windmilling propeller.

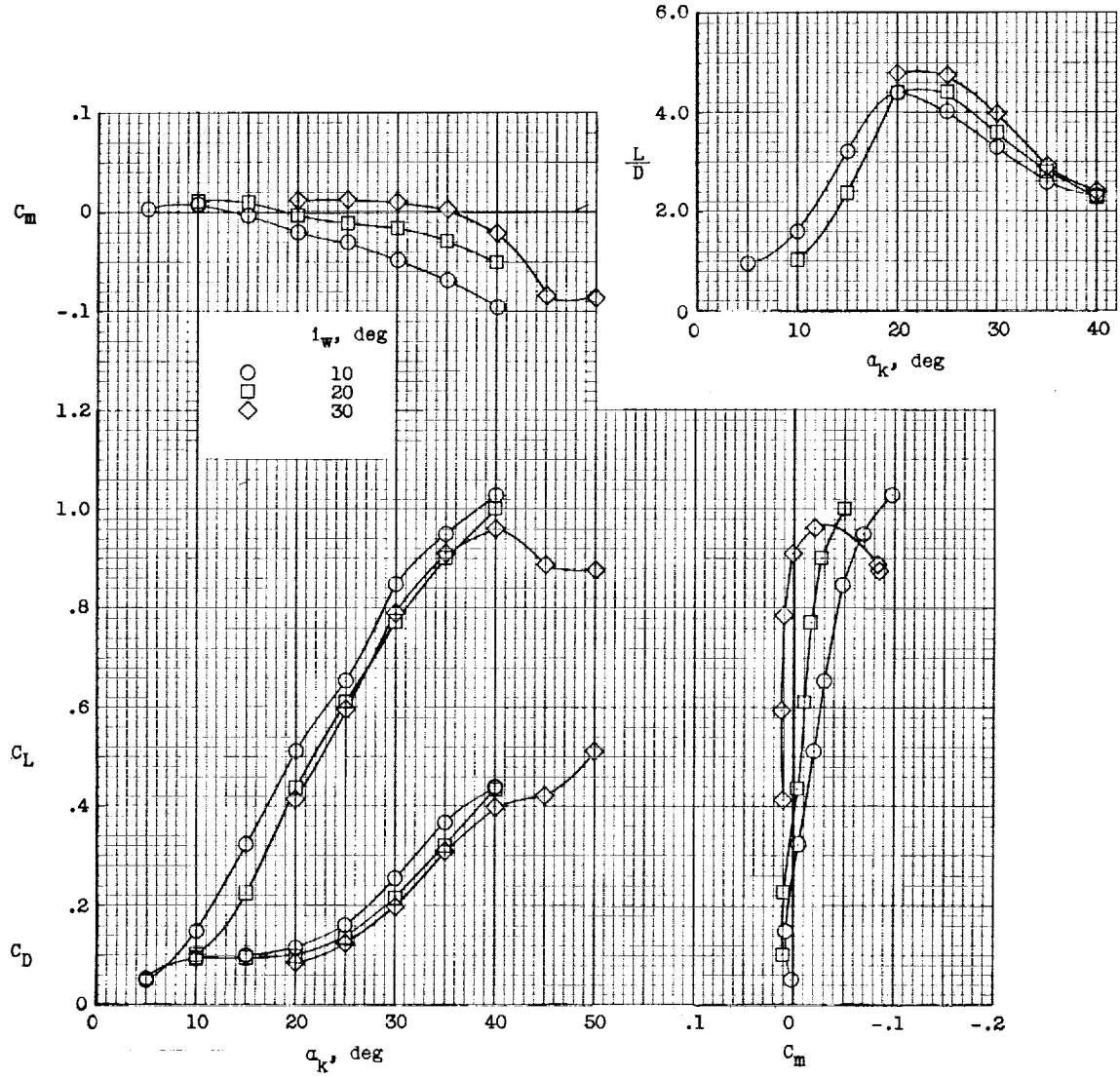

(b) Data plotted against keel angle.

Figure 8.- Concluded.

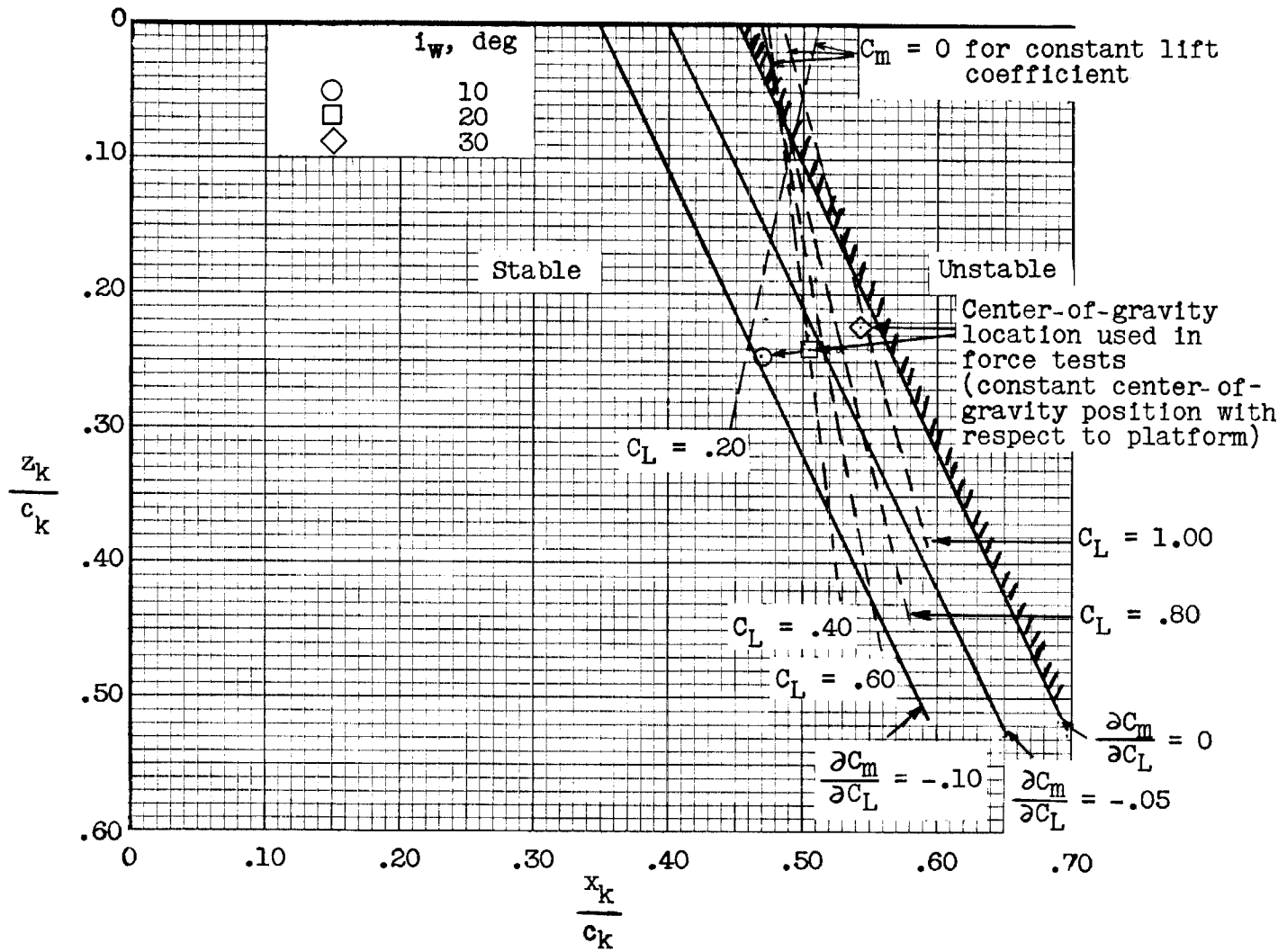

Figure 9.- Effect of center of gravity on static longitudinal stability and trim characteristics of the model. Windmilling propeller.

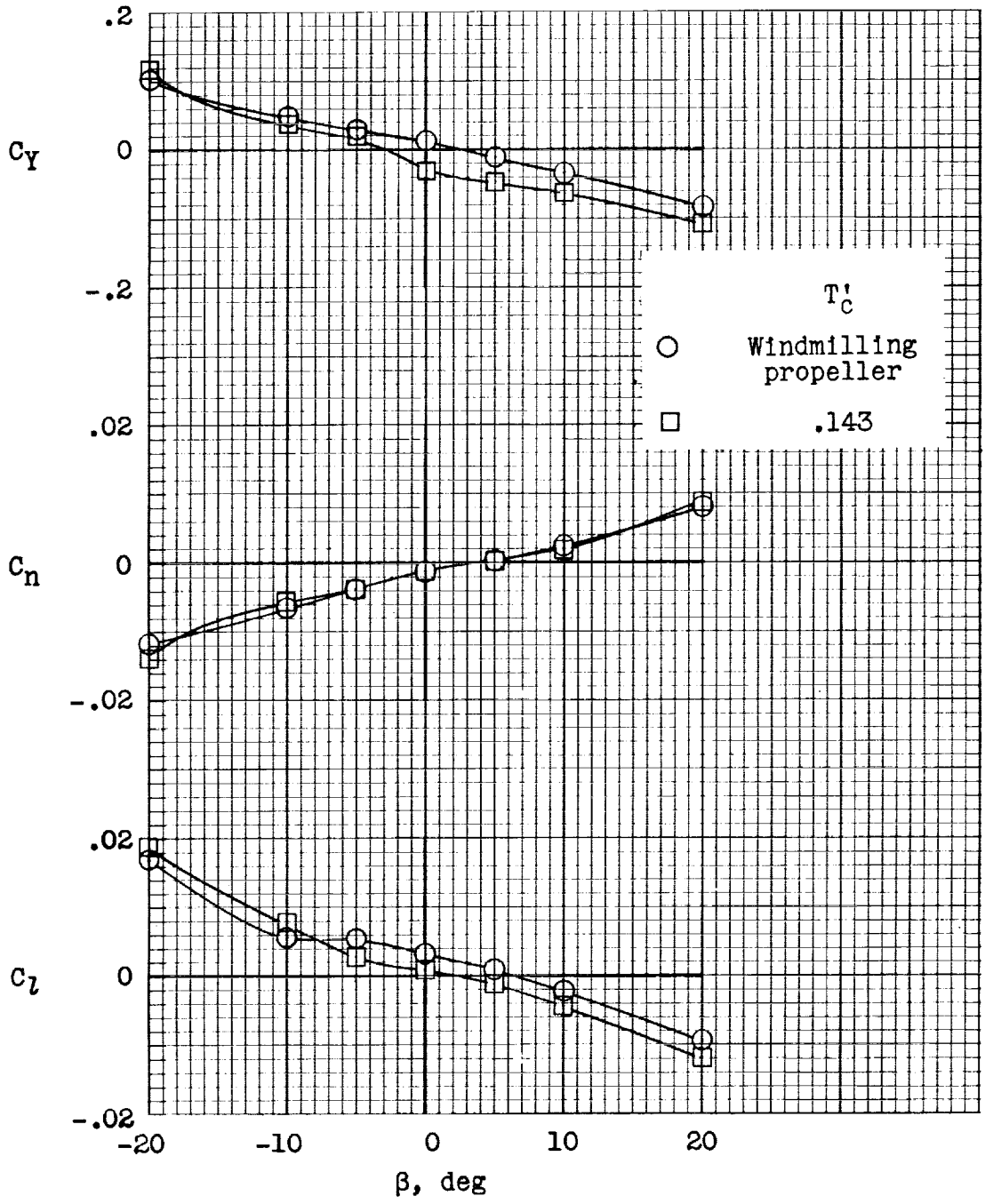

(a) $i_w = 10°$; $\alpha_p = 5°$.

Figure 10.- Static lateral characteristics of the model. Rudder off.

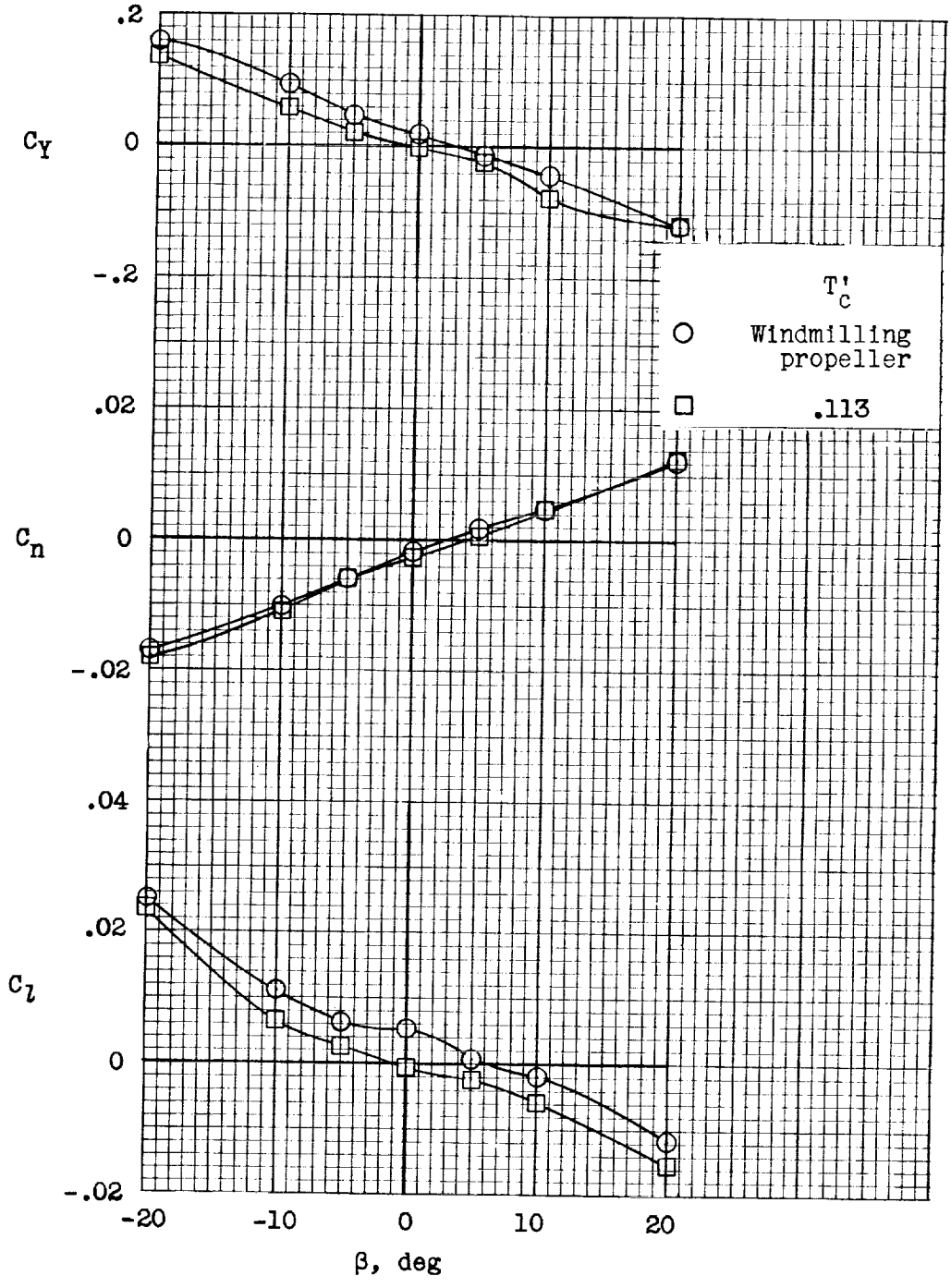

(b) $i_w = 20^o$; $\alpha_p = 0^o$.

Figure 10.- Continued.

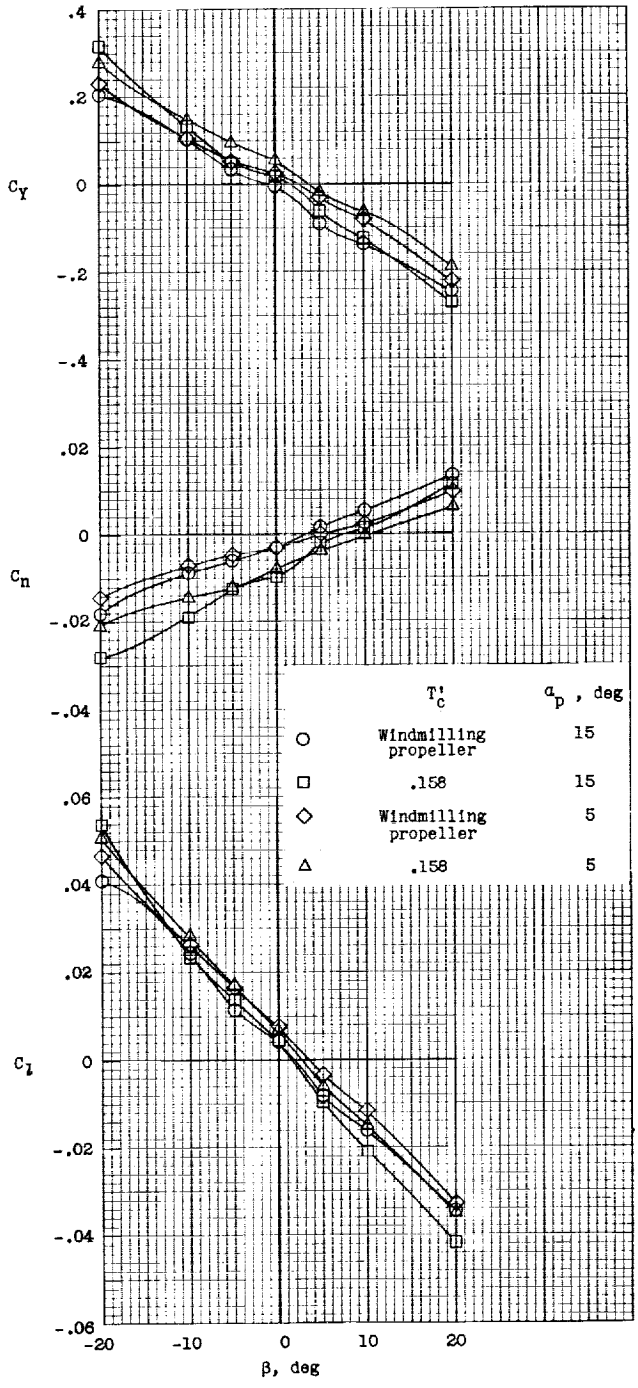

(c) $i_w = 30^o$.

Figure 10.- Concluded.

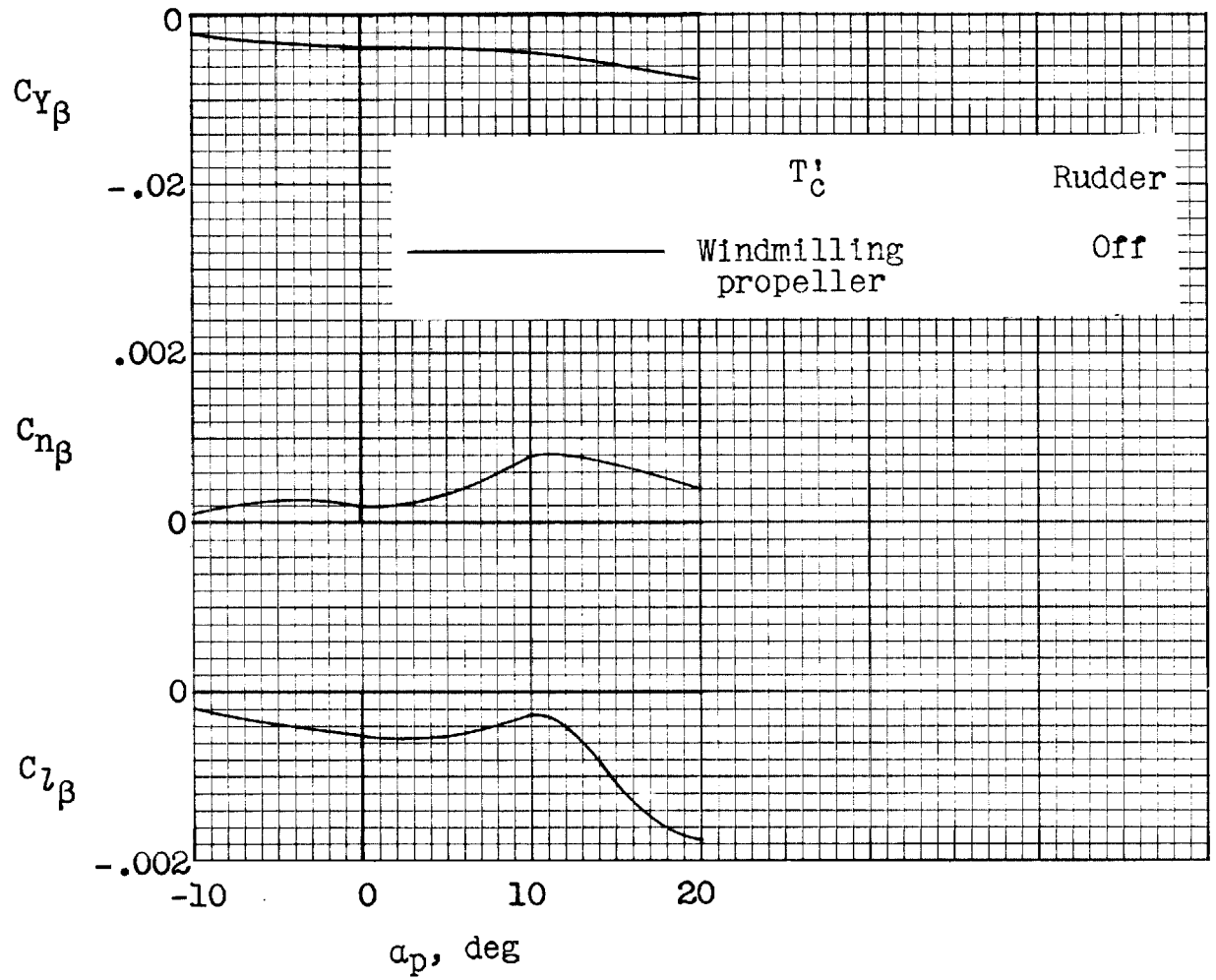

(a) $i_w = 10^o$.

Figure 11.- Static lateral stability parameters of the model. Windmilling propeller.

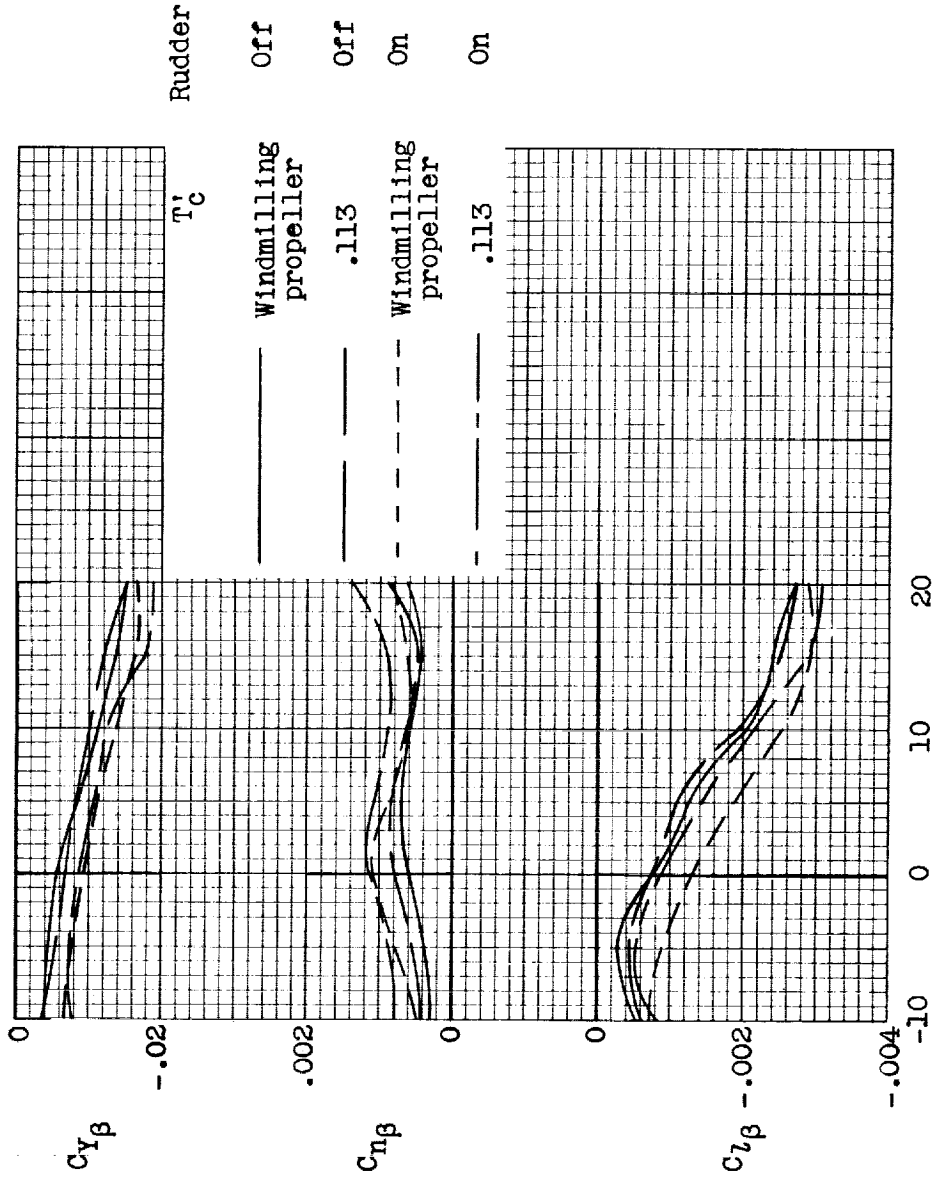

(b) $i_w = 20°$.

Figure 11.- Continued.

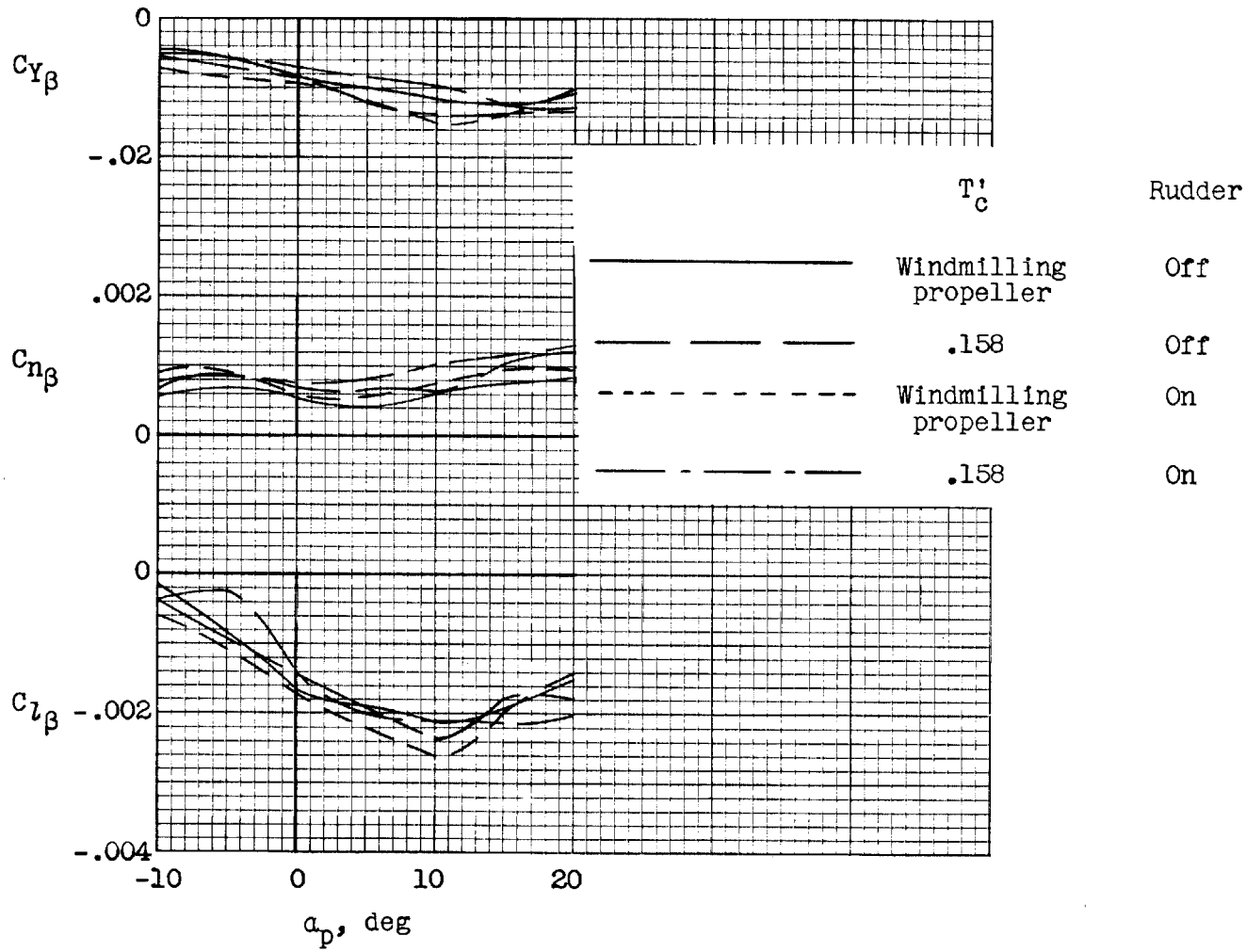

(c) $i_w = 30^\circ$.

Figure 11.- Concluded.

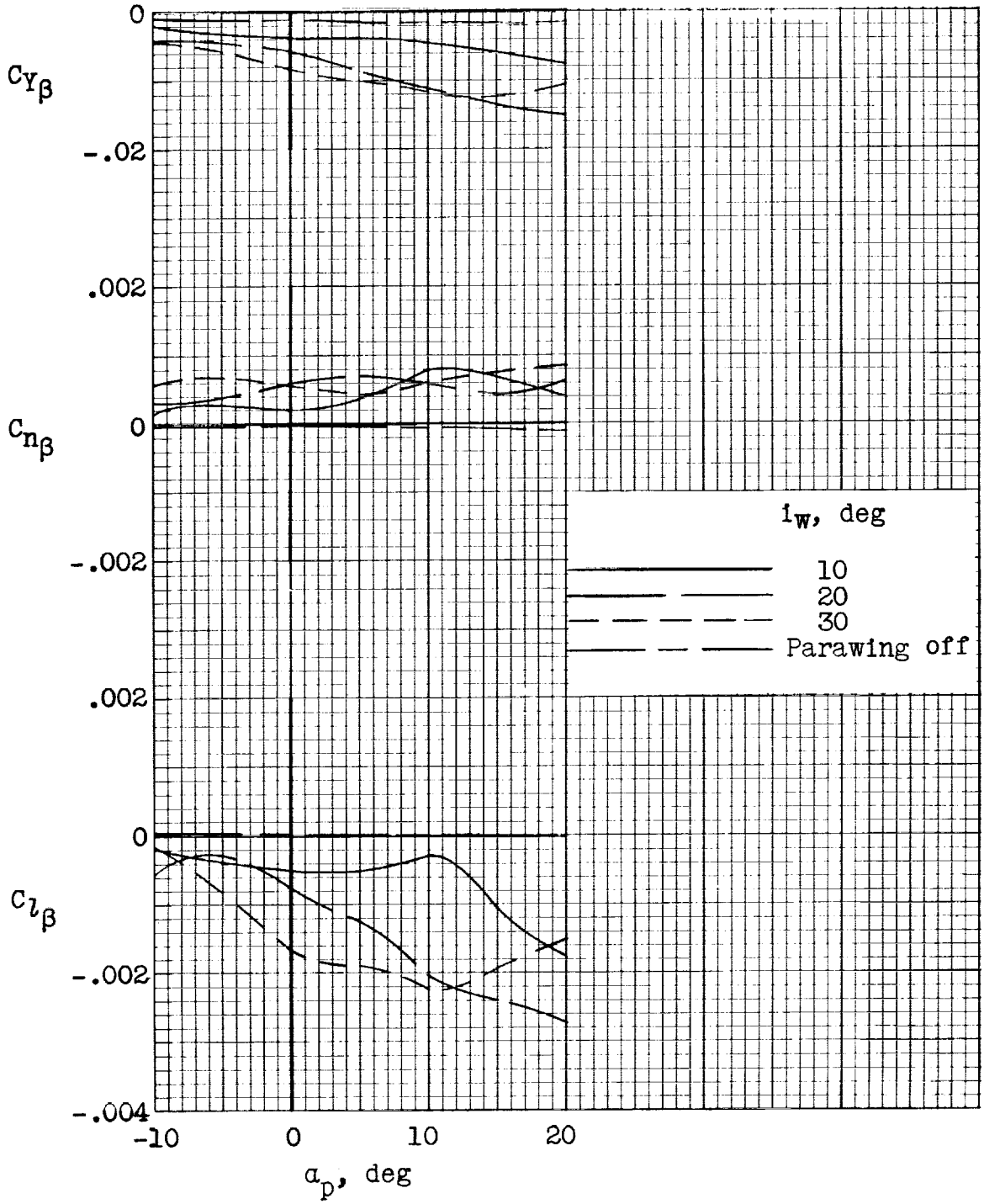

Figure 12.- Comparison of static lateral stability characteristics of the model. Rudder off. Windmilling propeller.

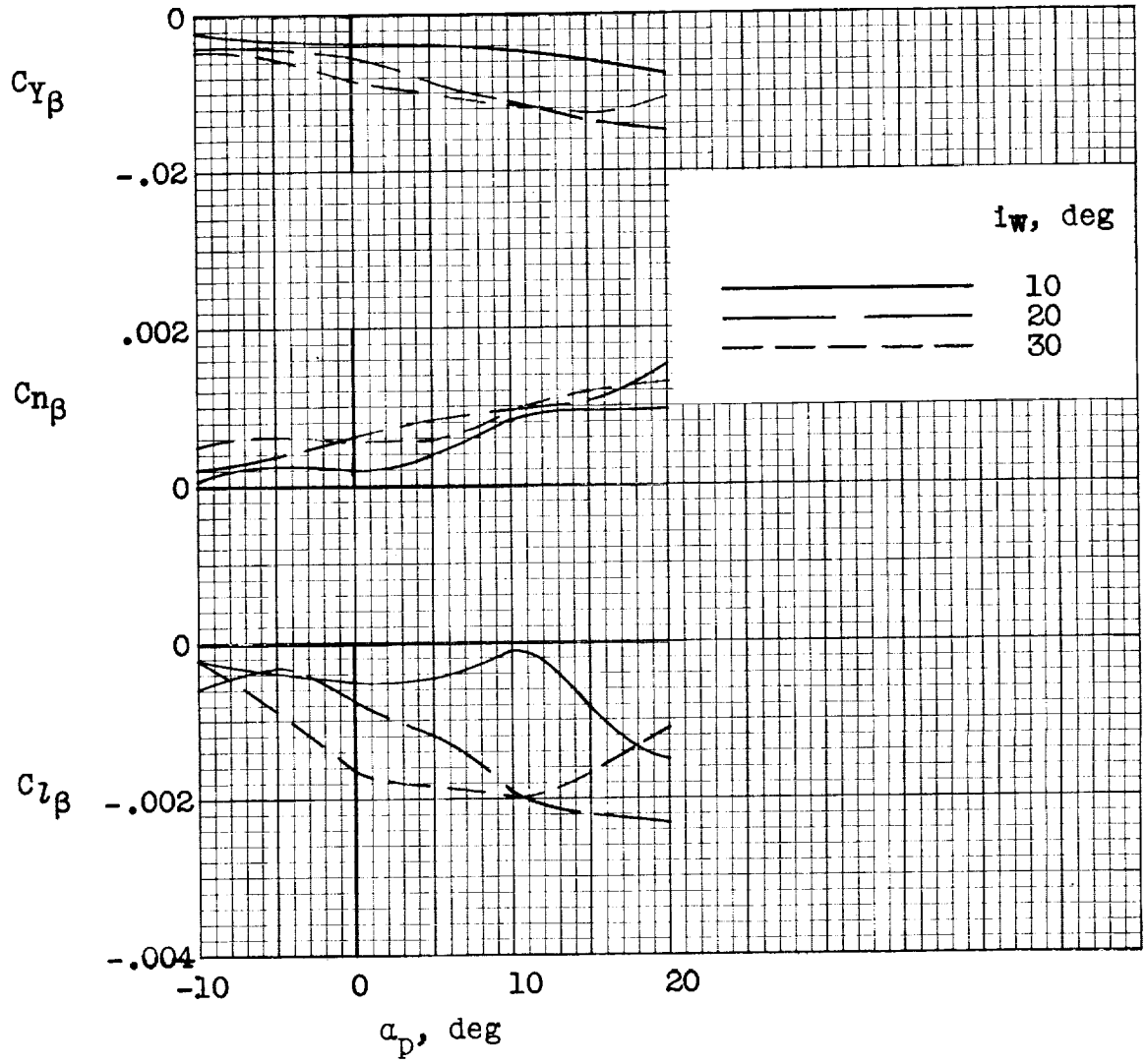

Figure 13.- Comparison of static lateral stability characteristics of the model. Data referred to stability axes, rudder off. Windmilling propeller.

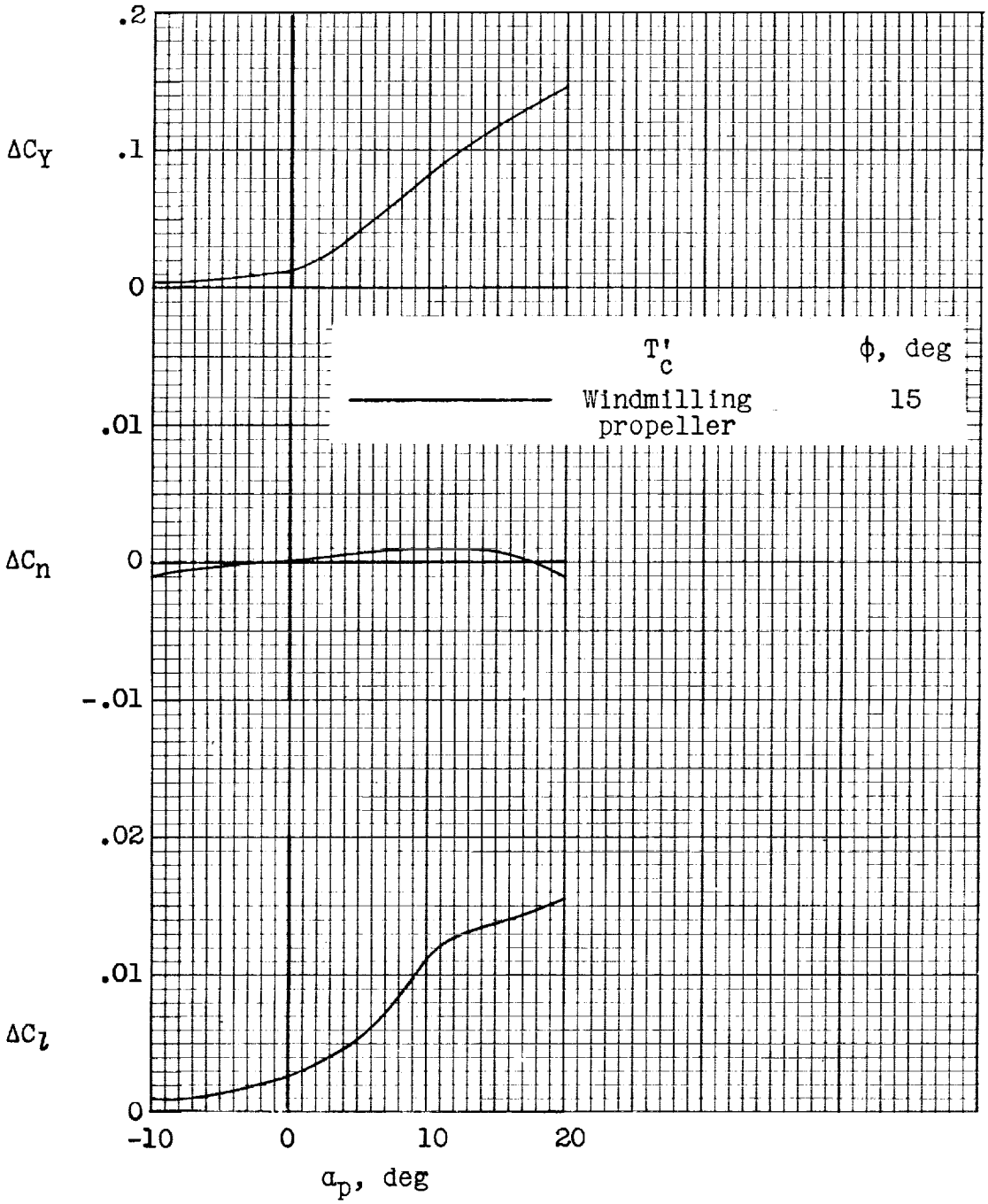

(a) $i_w = 10^o$.

Figure 14.- Incremental lateral forces and moments produced by rolling the wing.

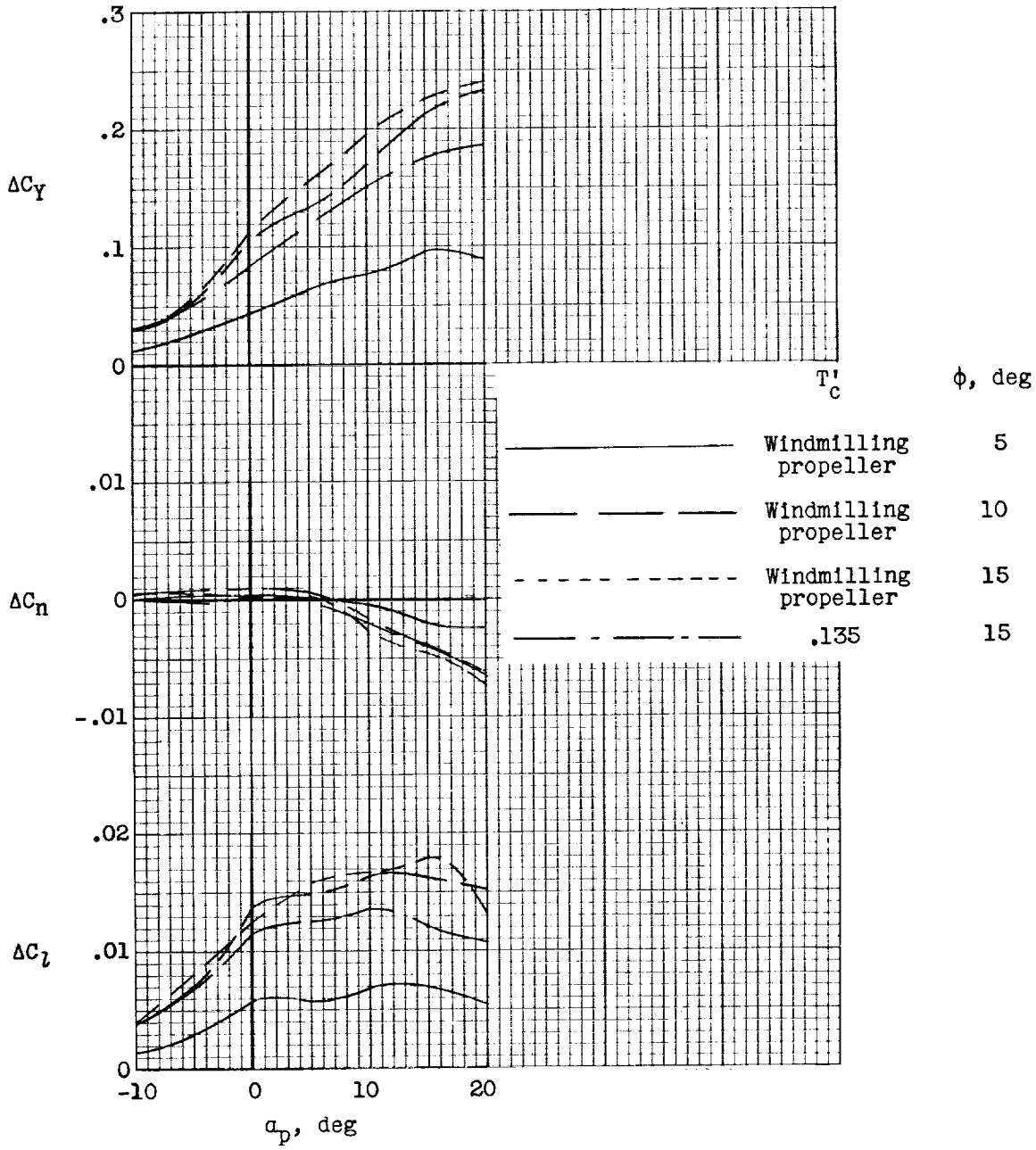

(b) $i_w = 20^\circ$.

Figure 14.- Continued.

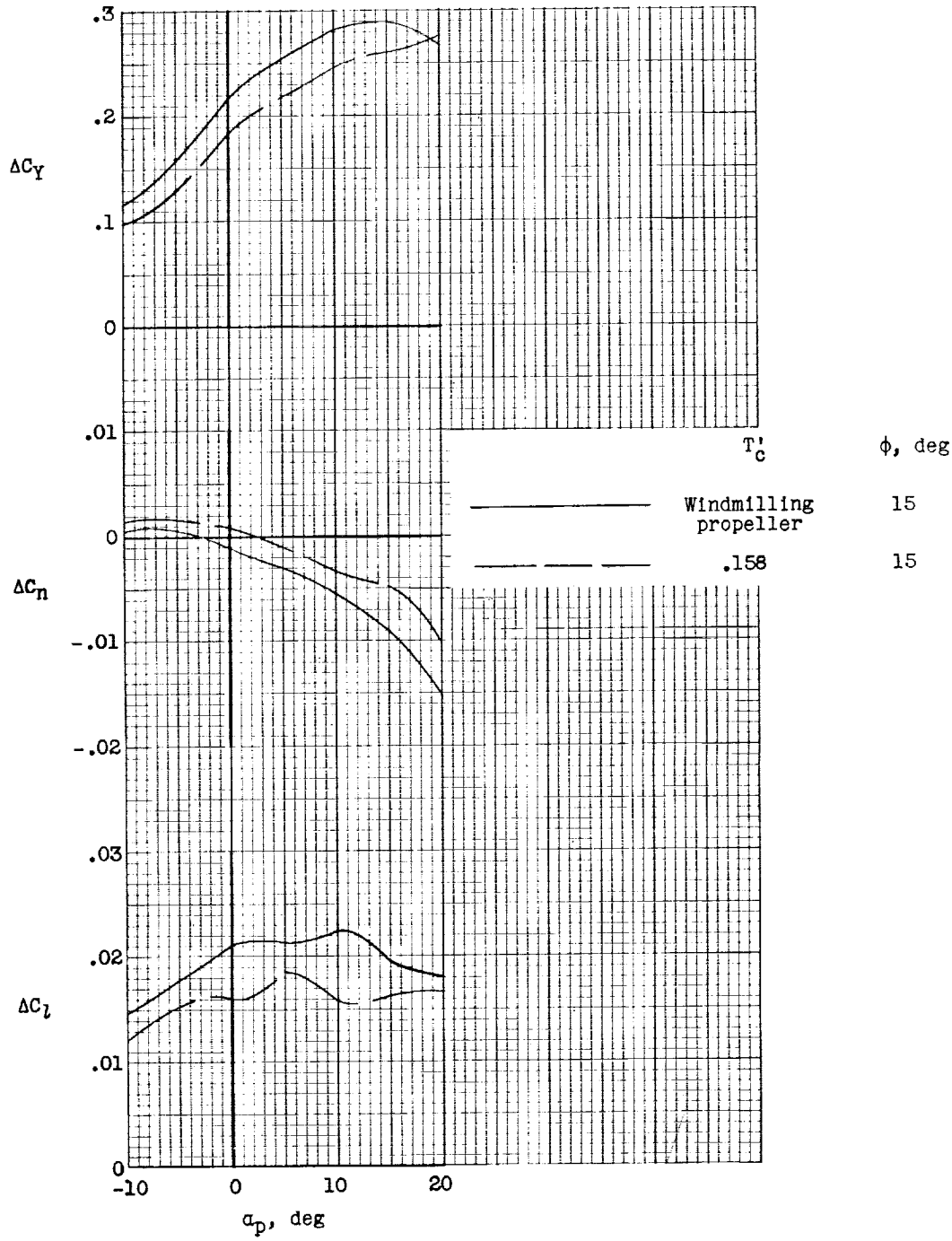

(c) $i_w = 30^o$.

Figure 14.- Concluded.

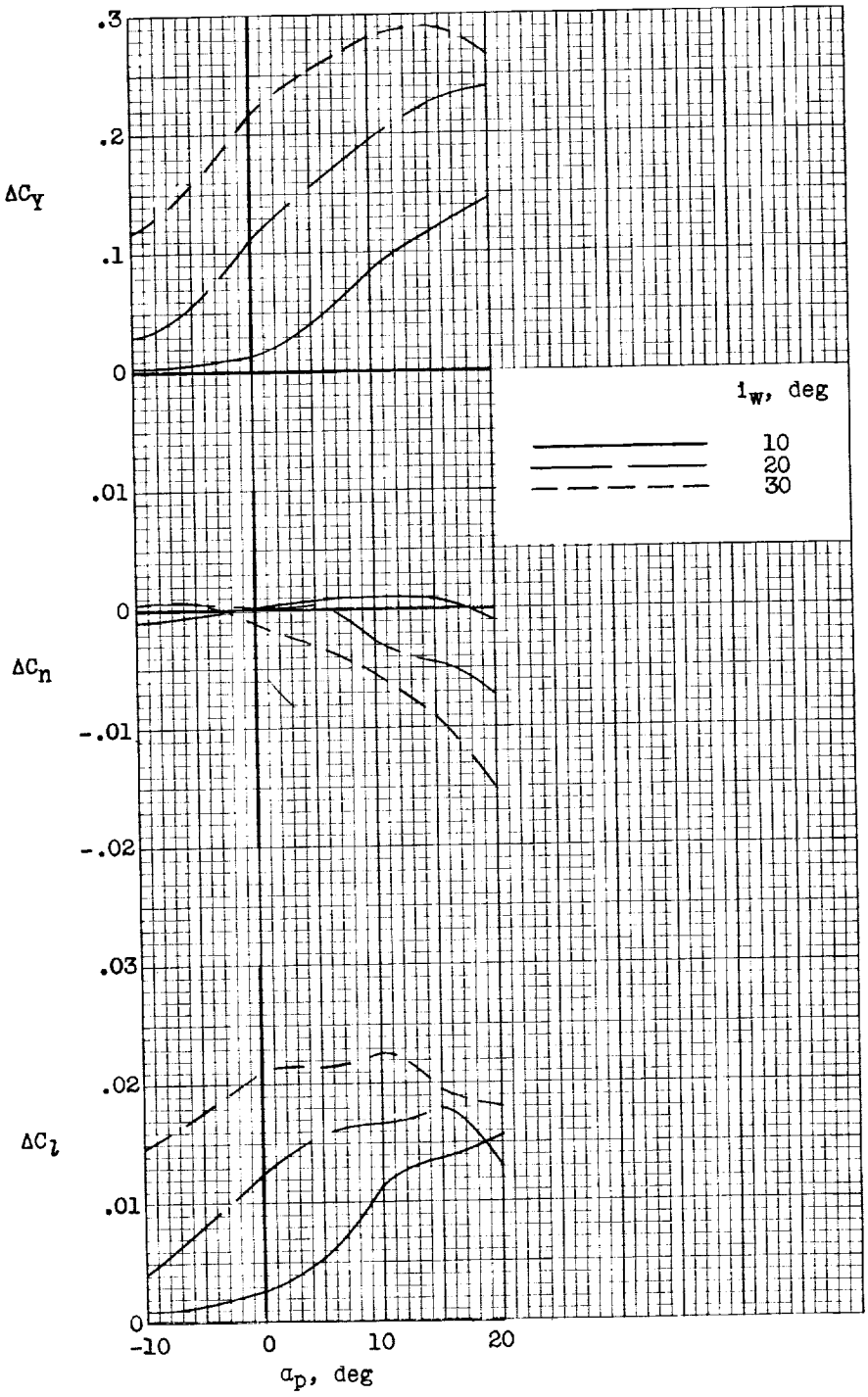

Figure 15.- Comparison of incremental lateral forces and moments produced by rolling the wing. $\phi = 15^{\circ}$. Windmilling propeller.

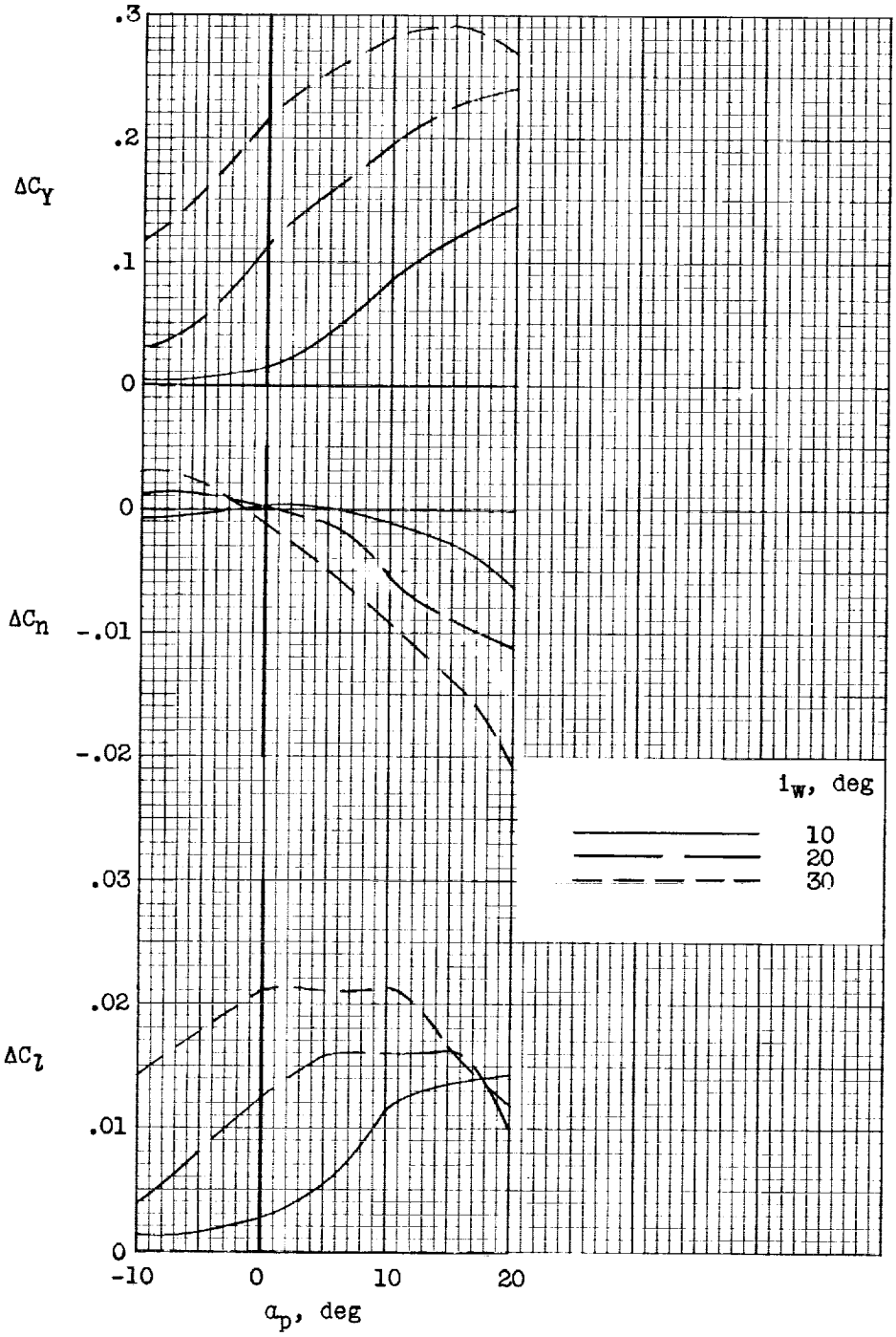

Figure 16.- Comparison of incremental lateral forces and moments produced by rolling the wing. Data referred to the stability axes. $\phi = 15^\circ$. Windmilling propeller.

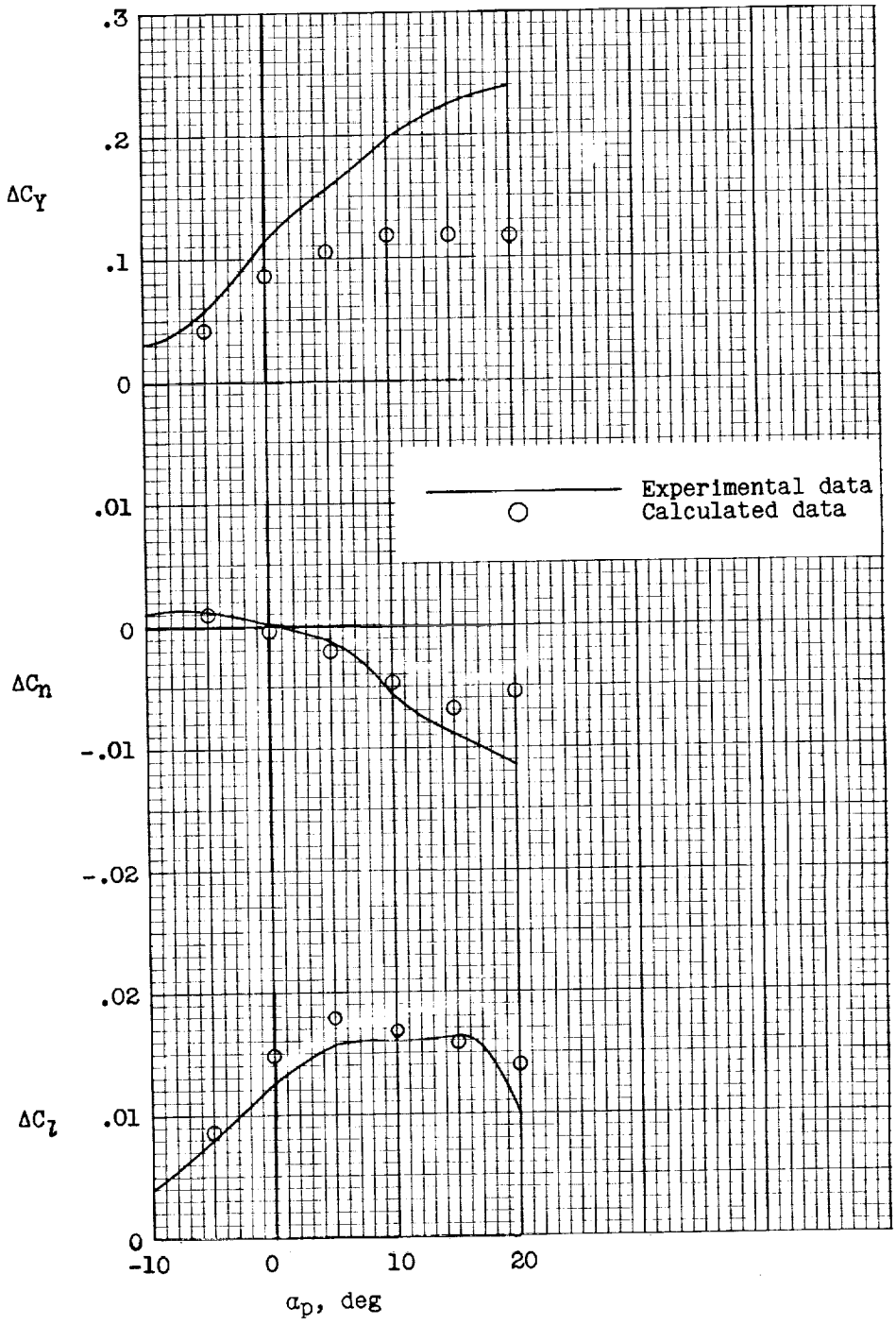

Figure 17.- Comparison of calculated and measured incremental lateral forces and moments produced by rolling the wing. $\phi = 15^\circ$. Windmilling propeller; $i_w = 20^\circ$.

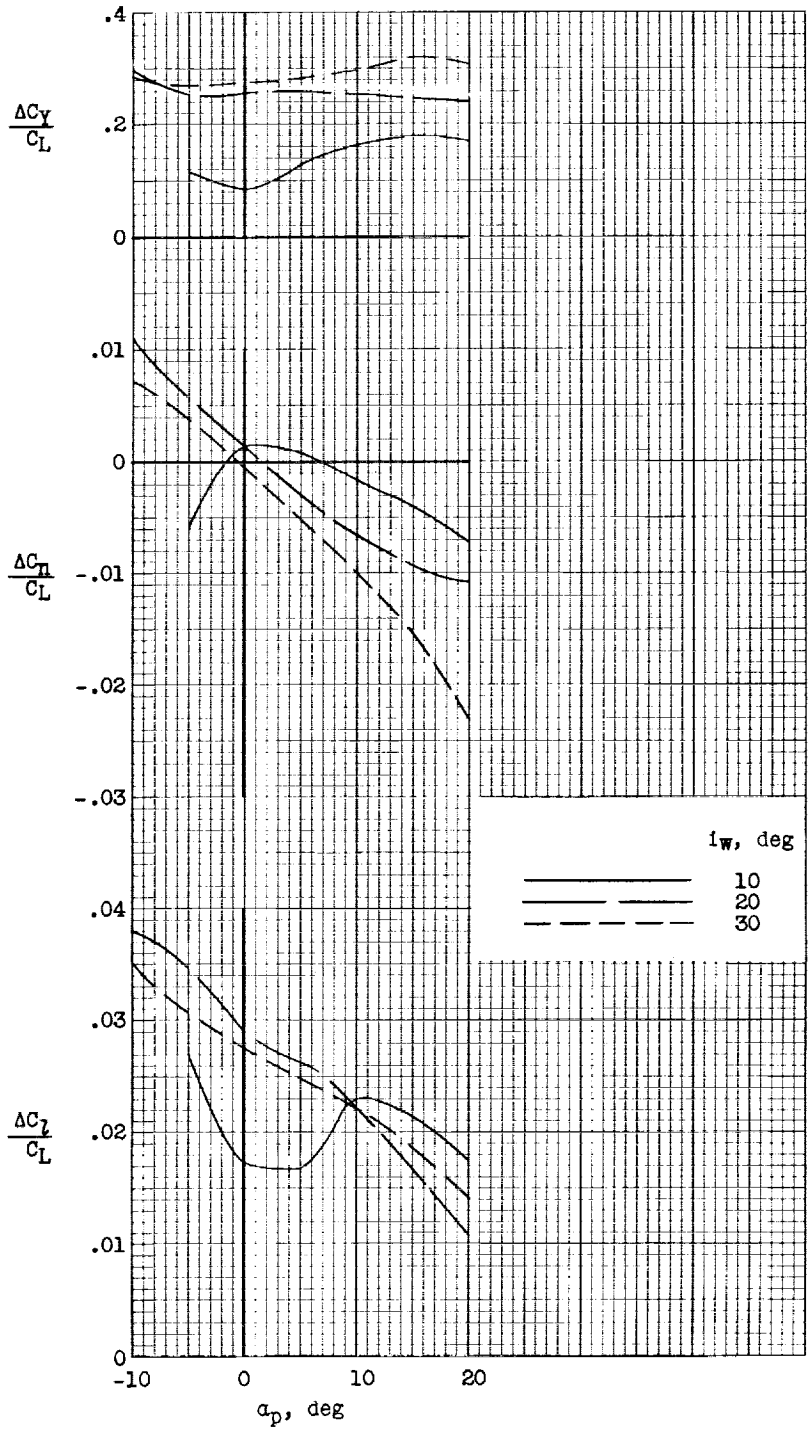

Figure 18.- Comparison of lateral control effectiveness parameters of the wing. $\phi = 15^{\circ}$. Windmilling propeller.

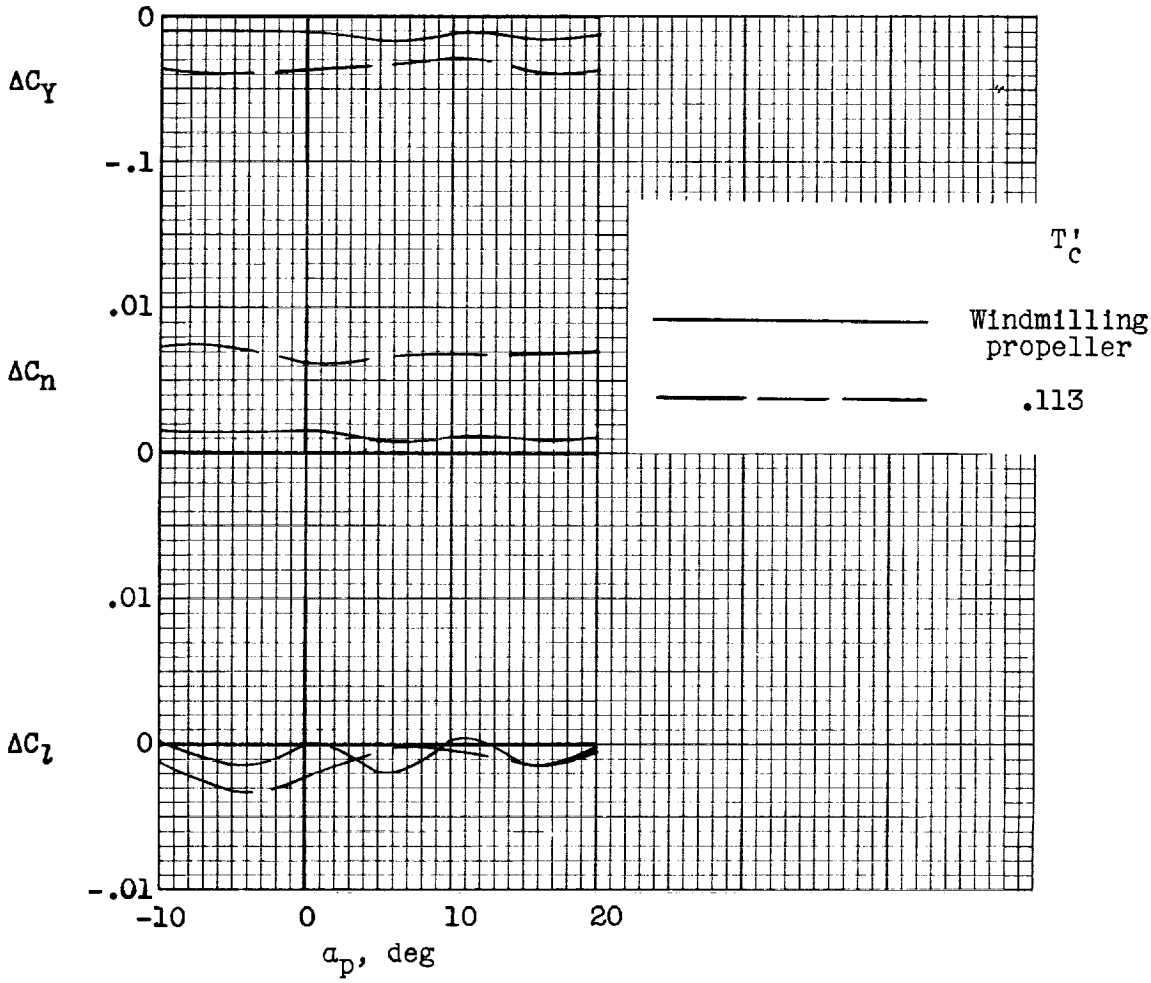

(a) $i_w = 20^\circ$; $\delta_r = 20^\circ$.

Figure 19.- Incremental lateral forces and moments produced by rudder deflection.

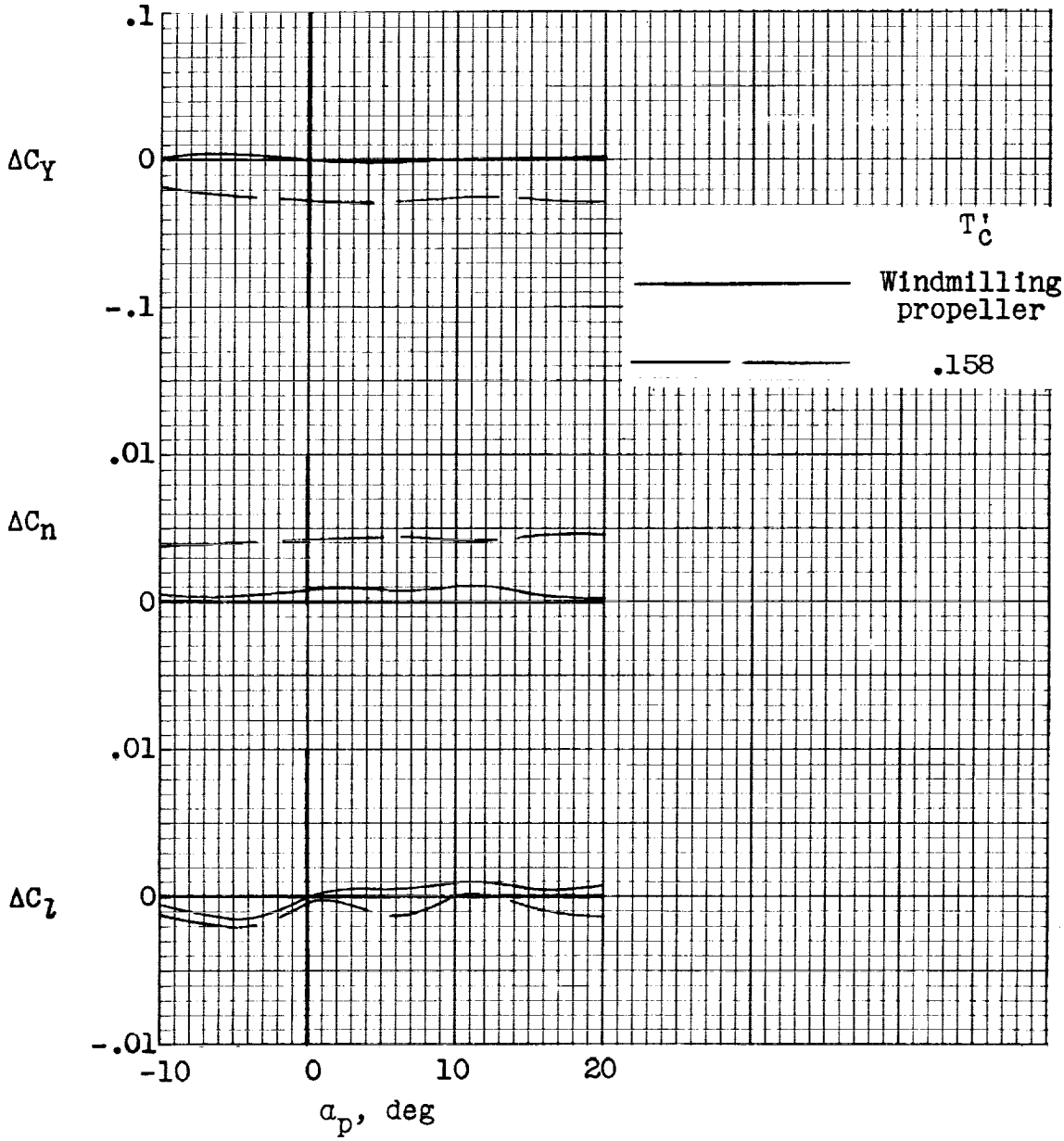

(b) $i_w = 30^o$; $\delta_r = 10^o$.

Figure 19.- Concluded.

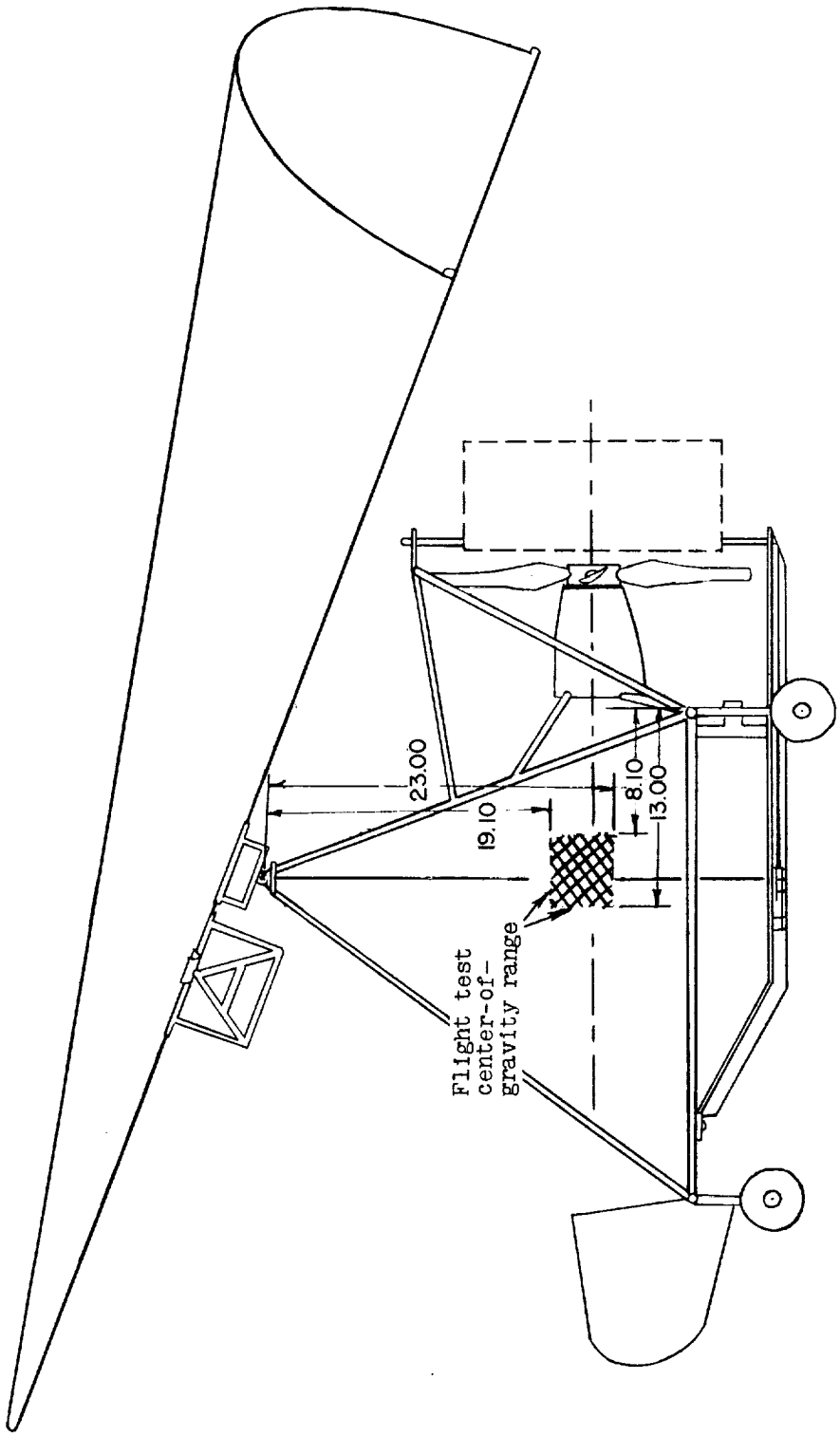

(a) Center-of-gravity range with reference to model platform.
Dimensions are in inches.

Figure 20.- Range of center-of-gravity locations used in the flight tests.

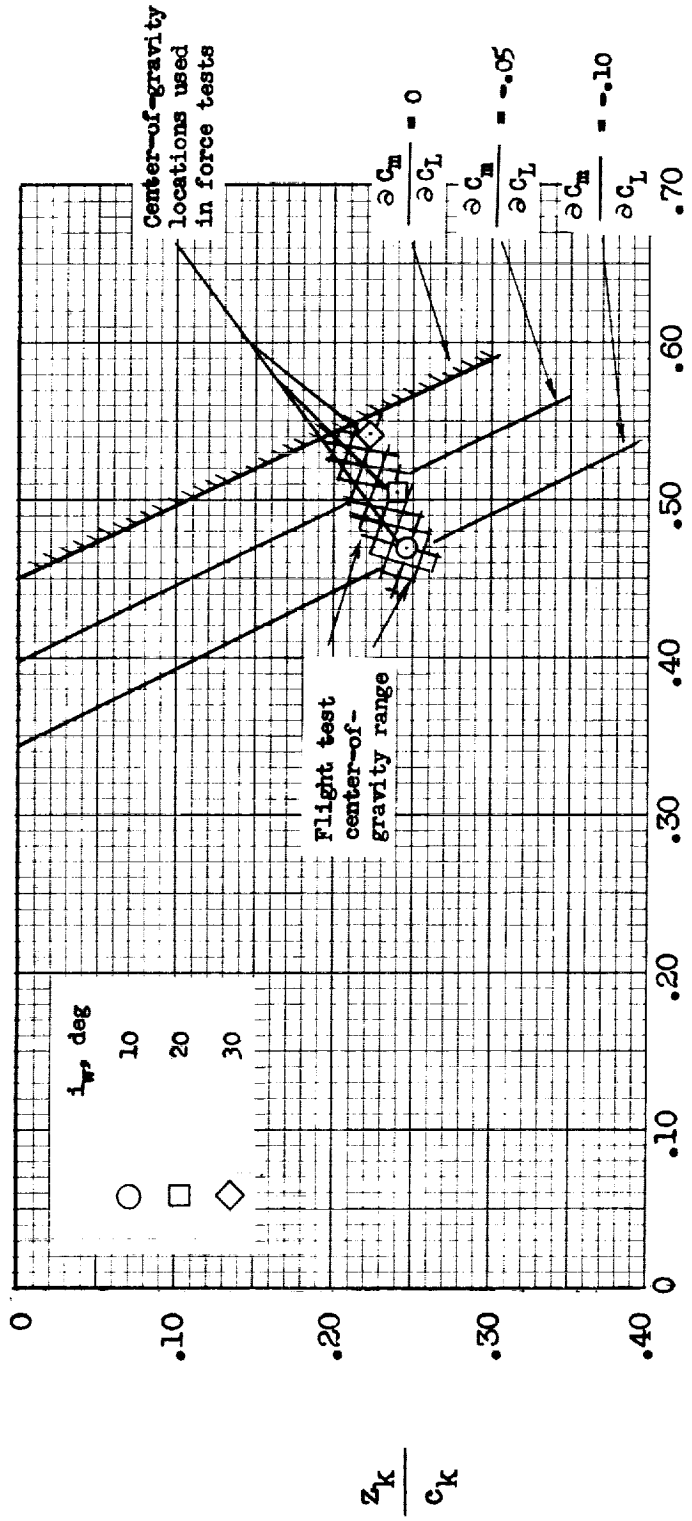

(b) Center-of-gravity range with reference to keel.

Figure 20.- Concluded.

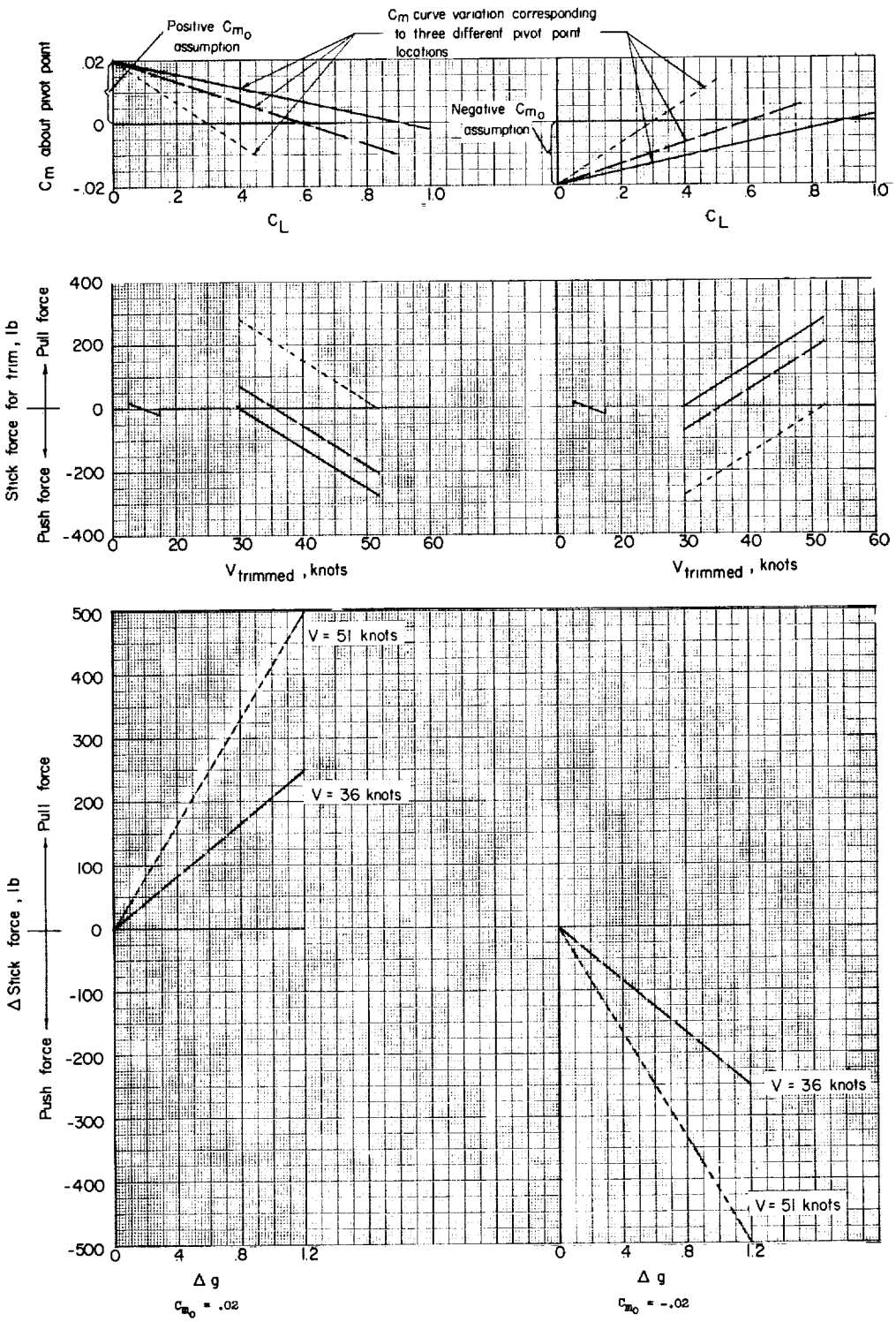

(a) Assumed longitudinal data.

Figure 21.- Hinge-moment and stick-force characteristics for a parawing utility vehicle.

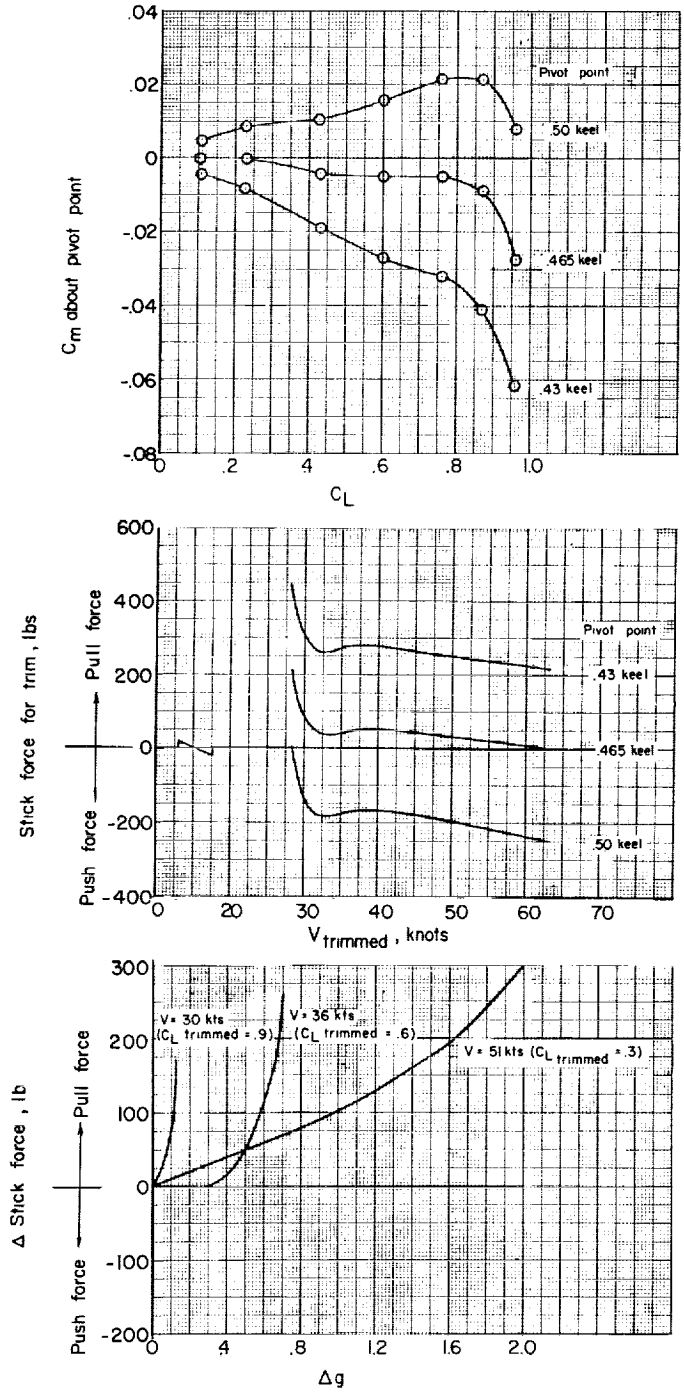

(b) Measured longitudinal data.

Figure 21.- Continued.

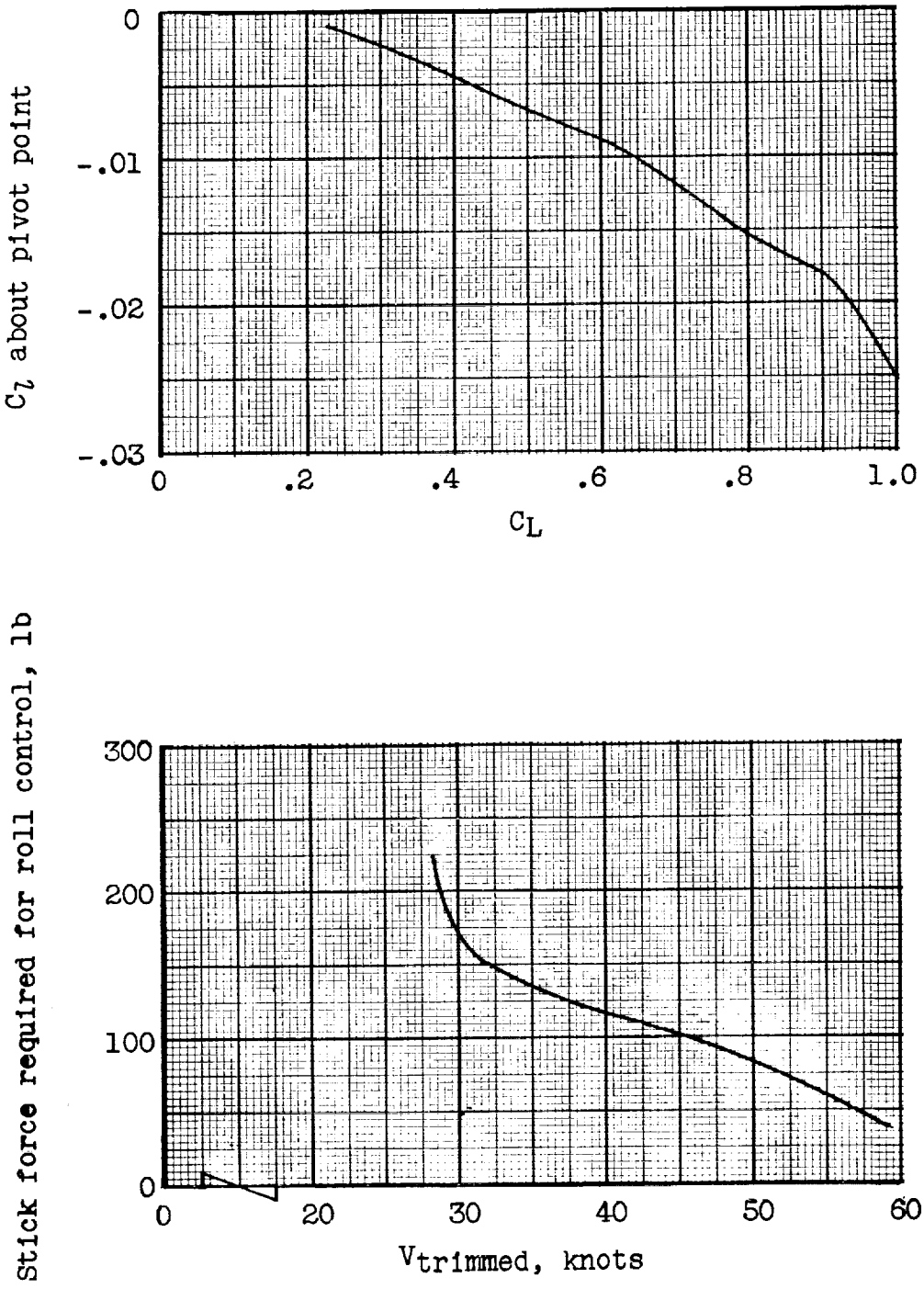

(c) Measured lateral data.

Figure 21.- Concluded.

NASA-Langley, 1962 L-1721